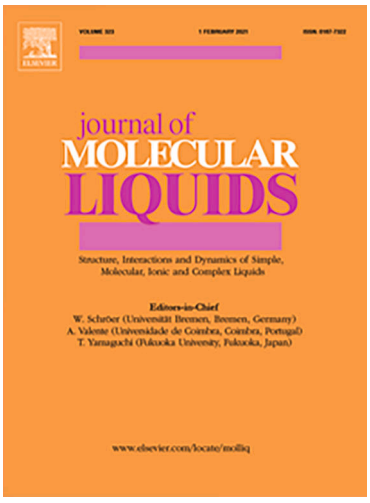


# High-Resolution investigation by Peltier-element-based adiabatic scanning calorimetry of binary liquid crystal mixtures with enhanced nematic ranges

J. Thoen, G. Cordoyiannis, P. Losada-Pérez, C. Glorieux

PII: S0167-7322(21)01928-0
DOI: https://doi.org/10.1016/j.molliq.2021.117204
Reference: MOLLIQ 117204

To appear in: *Journal of Molecular Liquids*

Received Date: 17 June 2021
Revised Date: 4 August 2021
Accepted Date: 7 August 2021

Please cite this article as: J. Thoen, G. Cordoyiannis, P. Losada-Pérez, C. Glorieux, High-Resolution investigation by Peltier-element-based adiabatic scanning calorimetry of binary liquid crystal mixtures with enhanced nematic ranges, *Journal of Molecular Liquids* (2021), doi: https://doi.org/10.1016/j.molliq.2021.117204

# High-Resolution investigation by Peltier-element-based adiabatic scanning calorimetry of binary liquid crystal mixtures with enhanced nematic ranges

J. Thoen[a,*], G. Cordoyiannis[b,c], P. Losada-Pérez[d], C. Glorieux[a]

[a] Laboratory for Soft Matter and Biophysics, Department of Physics and Astronomy, KU Leuven, Celestijnenlaan 200D, P.O. Box 2416, 3001 Leuven, Belgium
[b] Condensed Matter Physics Department, Jožef Stefan Institute, 1000 Ljubljana, Slovenia
[c] Faculty of Mechanical Engineering, Czech Technical University in Prague, 16000 Prague 6, Czech Republic
[d]Experimental Soft Matter and Thermal Physics Laboratory, Department of Physics, Université Libre de Bruxelles, Boulevard du Triomphe, CP223, 1050 Brussels, Belgium
Corresponding author. E-mail address: jan.thoen@kuleuven.be (J. Thoen)

*Keywords*: liquid crystal mixtures, heat capacity, enthalpy, phase transition, first-order and second-order transitions, critical anomaly, eutectics, Halperin-Lubensky-Ma effect

ABSTRACT

High-resolution Peltier-element-based adiabatic scanning calorimetry (pASC) has been used to investigate the temperature dependence of the specific heat capacity and specific enthalpy of two mixture systems of the liquid crystal smectic $A_1$ compound 5-n-nonyl-2-(4'-isothiocyanatophenyl)dioxane-1.3 (9DBT), and one of the smectic $A_d$ compounds 4-n-octyloxy-4'-cyanobiphenyl (8OCB) and 4-nonyloxy-4'cyanobiphenyl (9OCB). For both mixture systems, measurements have been carried out over a large temperature range, from the crystalline solid phase over the smectic and nematic phases into the isotropic liquid phase. Both systems exhibit substantial, mixing-induced, enhanced nematic ranges and large changes in the composition dependence of the transition temperatures between the different phases. In both systems, eutectic melting points have been located and, for the different mixtures, the melting and eutectic transition heats have been obtained. The nematic to isotropic (NI) transitions are weakly first order with latent heat values in the range usually observed for this transition in other liquid crystals. The critical behavior of the specific heat capacity at the NI transition is described by exponent values near the tricritical one of 0.5. Along the smectic A to nematic (AN) transition lines, strong composition dependence was observed for the latent heat, from almost zero to values comparable to those observed at the nematic to isotropic transition. The concentration dependence of these AN latent heats was adequately fitted with a crossover function consistent with a mean-field free-energy expression that has a nonzero cubic term; the latter is induced by the Halperin-Lubensky-Ma coupling between the smectic A order parameter and orientational order director fluctuations. The fitting analysis resulted in the location of a Landau-tricritical point along one branch of the transition line in the system 9DBT-8OCB and one in each branch (for low and high 9OCB mole fractions) of the NA transition line of the 9DBT-9OCB system. The effective critical exponent values for the specific heat capacity of the AN transitions follow the McMillan ratio-dependence observed for other liquid crystal mixtures.

## 1. Introduction

The study of phase transitions and the differences between related phases is an important aspect of condensed matter research, not the least in soft matter systems. In particular, liquid crystals have played and are playing a major role because of exhibiting many mesophases with symmetries between the ones of a crystalline solid and an isotropic liquid. These liquid crystalline phases possess orientational order but no or reduced positional order **[1-3]**. The

discontinuous (i.e. first-order) or continuous (i.e. second-order) nature and the universality class of the different phase transitions have been the object of extensive studies by many different techniques **[4-12]**.

The most frequently observed transition occurs between the normal isotropic (I) liquid phase and the nematic (N) phase; the latter exhibits only orientational and no positional order **[1]**. A more ordered phase is the smectic A phase, which, in addition to orientational order, exhibits also one-dimensional positional order (layered structure). Additional smectic phases (e.g. smectic B) with increased positional order (e.g. in the layers) can be also observed. Moreover, substantial differences have been observed between different types of smectic A, depending on the specific types of layered structure. For the simplest case, the layer thickness ($d$) is commensurate with the molecular length ($l$); this is the so-called smectic $A_1$ phase. When the layer thickness is twice the molecular length ($d \sim 2l$), the phase is referred to as smectic $A_2$. Furthermore, a phase quite often observed in polar compounds is the smectic $A_d$, with a layer thickness between the ones of smectic $A_1$ and smectic $A_2$ **[13]**.

Progress in liquid crystal phase transition studies has benefitted substantially from investigations imposing external experimental parameters (e.g. pressure, magnetic/electric fields, but even more so by mixing different liquid crystal compounds (quite often members of the same homologous series) and by mixing with non-mesogenic liquids or solid (nano)particles. Quite substantial variations in (usually binary) mixture phase diagrams have been encountered, from systems with injected smectic **A** phases to induced or enhanced nematic phases, resulting in various shapes of the temperature versus concentration curves and widths of nematic and smectic ranges **[14-16]**. Apparently, the width of the nematic range plays an important role in the order of the nematic-to-smectic A (AN) transition. Thus, many studies by means of various methods, in particular calorimetry, have focused on this transition. So far, the majority of high-resolution calorimetric studies have been carried out in binary mixtures with both compounds exhibiting smectic $A_d$ or smectic $A_1$ phases and always with compounds of the same homologous series **[17-26].** In a few cases, a non-mesogenic liquid was added to a liquid crystal compound **[16, 27-29]**.

Given that intermixing of systems with different smectic *A* layer types can result in unusual phase behavior, we have decided to study by high-resolution adiabatic scanning calorimetry mixture systems consisting of the smectic $A_1$ compound 5-n-nonyl-2-(4'-isothiocyanatophenyl)dioxane-1.3 (9DBT) on one side and the smectic $A_d$ compounds 4-n-octyloxy-4'-cyanobiphenyl (8OCB) or 4-nonyloxy-4'cyanobiphenyl (9OCB) on the other side. Both systems belong to different homologous series and exhibit substantial mixture-induced nematic range enhancement and substantial AN phase transition temperature dependences, as well as possibly eutectic behavior at melting **[30, 31]**.

## 2. Theoretical background

### *2.1 Isotropic to nematic and isotropic to smectic A transitions*

The only difference between the isotropic and the nematic phase is the orientational order of the long molecular axes in the latter. The description of this orientational order requires the introduction of a second-rank tensor **[1-3]**. For uniaxial symmetry this tensor can be diagonalised and the nematic phase can be described by a scalar order parameter. In the vicinity of the nematic-isotropic (NI) transition at $T_{NI}$ the thermodynamic behavior is usually described

by the Landau-de Gennes mean-field theory. One writes the free energy $F$ as an expansion of the order parameter $S_N$,

$$F = F_0 + \frac{1}{2}A_0 S_N^2 - \frac{1}{3}B_0 S_N^3 + \frac{1}{4}C_0 S_N^4 + \frac{1}{6}E_0 S_N^6 \quad (1)$$

In Eq. (1) $B_0 > 0$ and $A_0 = a_0(T - T^*)/T_{NI}$ with $a_0 > 0$ and $T^*$ the stability limit of the isotropic phase. $S_N = 0$ and $F = F_0$ in the isotropic phase. The presence of the cubic term leads to a finite order parameter discontinuity $S_{NI} = 2B_0/3C_0$. The excess heat capacity in the nematic phase is given by **[1, 32]**

$$C_p = \frac{a_0^2}{C_0 T_{NI}}\left[1 + \frac{B_0}{2(a_0 C_0)^{1:2}}\left(\frac{T^{**} - T}{T_{NI}}\right)^{-1/2}\right] \quad (2)$$

with $T^{**}$ the stability limit of the nematic phase. At the NI transition there is a jump in $C_p = 2a^2{}_0/C_0 T_{NI}$. For the enthalpy discontinuity (latent heat) one obtains

$$\Delta H_L = H_I - H_N = \frac{2a_0 B_0^2}{9C_0^2}. \quad (3)$$

Because of the presence of a (small) cubic term in Eq. (1), the NI transition is expected to be a weakly first-order one. Since at the direct transition from the smectic A to the isotropic phase (AI) the orientational order parameter becomes zero, this transition is also expected to be first order. Since both the orientational- and the positional order disappear, the AI transition involves a larger amount of latent heat **[32]**.

*2.2 Smectic A to nematic transition*

In addition to orientational order, the smectic A phase exhibits also one-dimensional positional order. The first theoretical proposals to describe the simultaneous existence of orientational and positional order resulted in the mean-field molecular models of Kobayashi **[33]** and McMillan **[34]**. As demonstrated by de Gennes **[35, 36]** the basic aspects of these models could be represented by a Landau free energy expansion with an additional coupling between the nematic and smectic order parameters. The smectic free energy $F_{NA} = F - F_N$ (with $F_N$ the nematic free energy) can be written as

$$F_{NA} = \frac{1}{2}a_0^*(T)|\psi|^2 + \frac{1}{4}c_0|\psi|^4 + \frac{1}{6}e_0|\psi|^6 - d_0|\psi|^2\delta S_N + \frac{1}{2\chi}\delta S_N. \quad (4)$$

For $T > T_{NA}$, one has $\delta S_N = S_N - S_{N0}$, with $S_{N0}(T)$ the nematic order parameter in the absence of smectic order. The temperature dependence of $a_0^*$ is given by $a_0^*(T) = \alpha_0(T - T_0)$. $\chi$ is the temperature-dependent nematic susceptibility which is larger near $T_{NI}$ and decreases with distance from the NI transition. The quantities $\alpha_0$, $c_0$, $e_0$, $d_0$, and $\chi$ are all positive constants. Minimizing $F$ with respect to $\delta S_N$ and eliminating it from $F$ results in

$$F_{NA} = \frac{1}{2}a_0^*(T)|\psi|^2 + \frac{1}{4}c|\psi|^4 + \frac{1}{6}e_0|\psi|^6, \quad (5)$$

where $c = c_0 - 2d_0^2\chi$. For $c > 0$ one has a continuous (second-order) transition at $T_{NA}$, for $c < 0$ a first-order one. $c = 0$ goes along with a tricritical point at the crossover from second-order to first-order. If one assumes a finite coupling between the nematic director fluctuations and the smectic order parameter, as demonstrated by Halperin and coworkers **[37, 38]**, the NA transition is always first-order because of the appearance of a third-order term in $F_{NA}$. The free energy $F_{NA}$ can be written as **[39]**

$$F_{NA} = \frac{1}{2}A(T)|\psi|^2 - \frac{1}{3}B|\psi|^3 + \frac{1}{4}c|\psi|^4 + \frac{1}{6}E|\psi|^6, \quad (6)$$

where $A = a'(T - T_0)/T_0$ and $T_0$ differs from $T_{NA}$ and $B$, $E$ and $a'$ are > 0. At a Landau tricritical point (LTP) one has $c = 0$, e.g. at a specific mole fraction $x^*$ in a binary mixture. Assuming near the LTP $c = c_0(x - x^*)$ (with $c_0 < 0$ and $x$ the mole fraction), it can be shown **[37-39]** that the entropy discontinuity at the LTP $x^*$ is given by

$$\frac{\Delta S^*}{R} = \frac{1}{2}a'\left[\frac{B}{2E}\right]^{2/3} \quad (7)$$

Here $S$ is the entropy, which should not be confused with the nematic order parameter $S_N$ in Eq. (1). It can also be shown **[39]** that near the LTP the reduced entropy difference $s \equiv \Delta S/R$ (with $R$ the gas constant) at mole fraction $x$ is relate to $s^* \equiv \Delta S^*/R$ at $x^*$ in the following way:

$$\left(\frac{s}{s^*}\right) - \left(\frac{s}{s^*}\right)^{-1/2} = \frac{\hat{a}}{s^*}(x - x^*) = y - y^*, \quad (8)$$

With $\hat{a} = -\frac{3}{8}(a'c_0/E)$ and $y \equiv \hat{a}x/s^*$ *and* $y^* \equiv \hat{a}x^*/s^*$. Thus, this results in a universal crossover function for $s/s^*$.

*The smectic A to solid transition*

Many elements or substances that are fully miscible in liquid solutions are often not so in the solid phase. An important miscibility condition for a complete range of solid solutions of two compounds A and B, is that they have the same type of crystal structure, which remains the same for the solution with the lattice sites being occupied largely at random by the two kinds of atoms or molecules. More often, because of differences in crystal structure or from differences in atomic or molecular size or shape or electronic properties, lattice incompatibility results in limited ranges of solubility, or in complete immiscibility. The analysis of the Smectic A-solid transition in mixtures of 9DBT with 8OCB or 9OCB in reference **[30]** did not study eutectic behavior. However, the reported shape of the Smectic A-solid transition line for 8OCB+9DBT suggests an interesting miscibility behavior for these compounds worth being further investigated.

## 3. Experimental

*3.1 Adiabatic scanning calorimetry: principle of operation.*

Adiabatic scanning calorimetry (ASC) was developed to obtain simultaneously and continuously the temperature evolution of the heat capacity $C_p$ and the enthalpy $H$ of a sample under investigation **[40-42]**. The key point of the ASC concept is to apply constant heating or

cooling power to a sample holder containing the sample. In an ASC, the sample holder is placed inside a surrounding adiabatic shield. In a heating run, the heat exchange between the shield and the sample holder is prevented by keeping the difference between their temperatures zero at all times. In a cooling run, the heat exchange is controlled and monitored. During a run the sample temperature $T(t)$ is recorded as a function of time $t$. Together with the applied power $P$ this directly results in the enthalpy curve

$$H(T) - H(T_0) = \int_{t_0}^{t(T)} P dt = P\left[t(T) - t_0(T_0)\right], \tag{9}$$

where $H(T_0)$ is the enthalpy of the system at temperature $T_0$ at the starting $t_0$ of the run. The heat capacity $C_p(T)$ is easily calculated via the ratio of the known constant power $P$ and the changing temperature rate $\dot{T} = dT / dt$,

$$C_p = \frac{P}{\dot{T}} \tag{10}$$

The specific values of the heat capacity $c_p$ and of the enthalpy $h$ are obtained by using the sample mass and the calibrated background values of the empty calorimeter and sample cells.

*3.2 Peltier-element-based adiabatic scanning calorimeter*

The practical implementation of ASC, in particular maintaining adiabatic conditions over long time and wide temperature ranges, is challenging. The 'classical' implementation, although quite successful in high-resolution studies of phase transitions **[16-18, 22, 27]**, is difficult to operate over extended temperature ranges and requires rather large samples (typically 0.5 g or more). Detailed descriptions of this kind of implementations can be found in **[40-42]** and references therein. However, in the past decade, this approach has been superseded by the development of the novel Peltier-element-based adiabatic scanning calorimeter (pASC), providing greater user-friendliness and requiring essentially smaller amounts of samples **[31, 43-47]**.

In **Fig. 1** a schematic representation of the central part of the pASC is given. The core of the device is a sample cell platform, equipped with an electrical heater and a sensitive resistance thermometer (typically a thermistor or platinum resistor). An airtight sample cell (e.g. a DSC crucible) is placed on the platform. The platform is soldered on the top plate of a Peltier element (PE), insuring a good thermal contact between them. The bottom plate of the PE is also in good thermal contact (soldered) with the adiabatic shield. Therefore, the PE acts as a differential thermometer for the temperature difference between the sample and the surrounding adiabatic shield. In a heating run, constant power is supplied to the heater near the sample holder, resulting in an increasing temperature of the sample, the sample holder and the platform. A proportional-integral-derivative (PID) control system (computer-controlled) delivers the necessary power to the heater on the adiabatic shield in order to keep the voltage output of the Peltier element zero and, thus, to maintain a zero temperature difference between the sample and the shield. In such a configuration, all the heat provided by the sample heater goes only to the sample and its addenda, hence the power $P$ in equations (9) and (10) is exactly known. In a cooling run, a fixed temperature gradient is imposed over the Peltier element. This leads to a constant amount of power drawn from the sample, which is measured by the Peltier element, now acting as a heat-flux sensor. In order to achieve temperature stability at the μK level, the adiabatic shield itself is surrounded by an additional thermal shield and a thermostat bath, each maintained at a lower temperature and controlled by PID control systems. To further improve

the adiabatic conditions, the internal volume of the calorimeter can be evacuated. More details regarding the pASC design can be found in **[44, 47]**.

*3.3 Materials and sample preparation*

The liquid crystals 8OCB and 9OCB were purchased from BDH. The 9DBT liquid crystal was purchased from WAT (Military University of Technology, Warsaw, Poland). The amount of each compound in the different mixtures was carefully weighted and thoroughly stirred prior to calorimetric measurements. Typically, 40 to 70 mg of samples were placed in stainless steel sample holders (Mettler-Toledo 120 µl medium pressure DSC crucibles) and hermetically sealed.

## 4. Results and discussion

*4.1 Phase diagrams and overview of the results*

In the following, in addition to the three pure compounds 9DBT, 8OCB and 9OCB, measurements are reported for eleven 8OCB+9DBT mixtures, as well as fifteen mixtures of 9OCB+9DBT. The mole fractions $x_{8OCB}$ for the different 8OCB+9DBT mixtures and the temperature of different phase transitions observed in the measuring range between 30 °C and 90 °C are listed in **Table 1**. Data for the 9OCB+9DBT system are given in **Table 2**. The corresponding phase diagrams are displayed in **Fig. 2**. The NI and AN transitions of pure 8OCB and 9OCB have not been measured again, since existing high-resolution calorimetric data **[22]** have been used and incorporated in further analysis. The phase diagram for 8OCB+9DBT is in good qualitative agreement with the one published by Czupryński *et al*. **[30]**. However, we did not observe the reported (relatively wide) coexistence range between the isotropic and smectic A phase for $x_{8OCB} < 0.2$. In addition, no values for the eutectic transition temperatures have been reported in **[30]**. The data displayed in the phase diagram for 9OCB+8OCB in **Fig. 2** and **Table 2** are new, so far not reported in literature. In both systems the nematic phase temperature range is enhanced in a certain part of the phase diagram, namely, for mole fractions between 0.5 and 0.7 of the nOCB compound. For mole fractions of the nOCBs below 0.2 the nematic phase is expelled and there is a direct AI transition, which is also the case for pure 9DBT. The enhancement of the nematic phase is mild for 8OCB+9DBT: from a nematic range $\Delta T_{nem}$ = 13.15 K for pure 8OCB to $\Delta T_{nem}$ =17.10 K for $x_{8OCB} = 0.733$. In the system 9OCB+8OCB the relative change is substantially larger: from $\Delta T_{nem} = 2.14$ K to $\Delta T_{nem} = 8.70$ K for $x_{9OCB} = 0.527$. In **Fig. 3** a typical set of the direct results for the specific heat capacity $c_p$ and specific enthalpy $h$ are presented for three different mole fractions of 8OCB (upper part of **Fig. 2**) of the binary system 8OCB+9DBT. For the three mixtures low temperature eutectic and melting transitions are encountered. For $x_{8OCB} = 0.111$ there is no nematic phase and a direct AI transition is observed. In the two other cases, NA transitions are revealed, albeit with quite small thermal signatures. Similar results are obtained for other mixture of 8OCB+9DBT, as well as for the mixtures of 9OCB+9DBT. Several aspects of these different phase transitions are discussed in the subsequent sections.

*4.2 Melting behavior*

Although the size and polarity are quite different between 9DBT and the two nOCBs in the investigated binary systems the two compounds are fully mixable in the I phase and in the two mesophases (N, smectic A). Apparently, the molecular mobility in these liquid phases allows enough positional and orientational adaptation. This is no longer the case in the solid phase,

where the two compounds fully separate via a eutectic process, as can be seen in the phase diagrams of **Fig. 2**. In the low temperature part (α) of these phase diagrams, precipitated solid 9DBT coexists with a liquid solution of the nOCB and 9DBT with increasing concentration of the nOCB with decreasing temperature. In part (β), one observes the inverse situation with the concentration of the solid nOCB increasing with decreasing temperature. In the (γ) part separated solid 9DBT and nOCB are present. The transition line separating the smectic A phase from the (α) or (β) region is usually referred to as *liquidus* and the transition line to the (γ) region as *solidus*. The different solidification processes result in substantial variations in the energy content of the mixtures. These are clearly visible in the temperature dependences of the effective specific heat capacity and enthalpy, which are simultaneously obtained by pASC (see, for instance, **Fig. 3**). The enthalpy results allow accurate determination of the enthalpy variation of the melting ranges, (α) or (β), for the different mixtures, as well as for the final solidification at the eutectic temperature. In Table 3 the resulting melting and eutectic enthalpy changes are summarized for 8OCB+9DBT. In Table 4 corresponding results are given for 9OCB+9DBT. In **Fig. 4** the data are displayed graphically for 8OCB+9DBT and 9OCB+9DBT, respectively. Both systems exhibit an eutectic point: at $T = 41.7 \pm 0.1$ °C and $x_{8OCB} = 0.585 \pm 0.005$ for 8OCB+9DBT ant at $T = 47.0 \pm 0.3$ °C and $x_{9OCB} = 0.422 \pm 0.005$ for 9OCB+9DBT.

Further insights in the melting and eutectic behavior can be achieved from the plot of $h(T)$ in **Fig. 5** for a set of mixtures of 8OCB+9DBT from the (α) side in **Fig. 2**. In this figure, the specific enthalpy has been normalized to a value of 160 J/g at 60 °C. Such a shift corresponds to an appropriate choice of $H(T_0)$ in Eq. (9). Equating the $h(T)$ values in the liquid smectic A phase leads to a clear view of the energetic situation in the solid and the two-phase region. It can immediately be verified that the eutectic transition always occurs at 41.7 °C, and it is sharp, regardless of the overall composition. In contrast, the melting temperature range of the solid (here 9DBT) in the two-phase region becomes very broad and decreases with concentration, finally disappearing at the eutectic point concentration. The eutectic transition enthalpy increases and the solid melting enthalpy decreases with increasing mole fraction.

*4.3 Nematic to isotropic transition*

As pointed out in section 2.1, the presence of a non-zero $B_0$ coefficient in Eq. (1) results in the first-order character of the nematic to isotropic transition. A consequence of this is the prediction of an enthalpy discontinuity at the NI transition (see Eq. (3)). This is also predicted for a direct smectic A to isotropic transition. From a detailed analysis, we have found, indeed, finite amounts of latent heat for all the mixtures. The obtained values are listed in Table 5 and in an overview graph in **Fig. 6**. As an example, the specific heat capacity and enthalpy curves near the NI transition are displayed in **Fig. 7** for the 8OCB+9DBT mixture with mole fraction $x_{8OCB} = 0.914$. For display reasons, a linear temperature dependent enthalpy increase (corresponding with a constant background heat capacity) has been subtracted from the original experimental enthalpy data.

From a comparison of the NI latent heat values with the ones for the melting behavior in **Fig. 4**, it follows that the NI values are almost two orders of magnitude smaller, confirming the very weakly first-order character of this phase transition. The direct AI values are substantially larger than the NI ones, but still an order of magnitude smaller than for melting. The smallness of the NI latent heats indicates that these transitions are close to second order and one might expect fluctuation effects resulting from many physical properties in exhibiting critical-point-

like behavior described by power laws with appropriate critical exponents. Indeed, this is also the case for the specific heat capacity $c_p$. The top part of **Fig. 7** gives the temperature dependence of $c_p$ near the NI transition of a binary 8OCB+9DBT mixture. The two dotted lines correspond to a narrow two-phase region of about 130 mK. The effective $c_p$ values in the two-phase region corresponding to the derivatives of the (slightly inclined) vertical piece of the enthalpy curve of the lower part of **Fig. 7**, are not included. The two-phase region is the result of the presence of some small amount of impurities that can never be completely eliminated.

For purely second-order (continuous) phase transitions, the limiting behavior of the specific heat capacity $c_p$ can be described by means of a power law of the form **[1, 32]**:

$$c_p = A|\tau|^{-\alpha} + B\,, \tag{11}$$

with $\tau = (T - T_c)/T_c$, $A$ the critical amplitude, $\alpha$ the critical exponent, $T_c$ the critical temperature, and $B$ the background term. In the mean-field approach, as expressed by Eq. (2), the value of $\alpha$ would be 0.5 when $T_c$ is identified with $T^{**}$. Power law fits with an equation of the form of Eq. (11) can be carried out for $c_p$ near the NI transition to arrive at critical exponent and amplitude values. However, fits with Eq. (11) must be made separately above and below $T_{NI}$ with different effective critical temperatures, $T^*$ and $T^{**}$, which are different for the first-order transition at $T_{NI}$. We have carried out fits with Eq. (11) for the data in **Fig. 7** below and above $T_{NI}$ separately with adjustable parameters $A$, $T^*$ (or $T^{**}$), $\alpha$, $B$. We found that the results depended strongly on the temperature range of the included data. When range-shrinking, $\alpha$ values changed from 0.35 to near 0.5 below $T_{NI}$ and from 0.3 to 0.4 above $T_{NI}$. Fitting the data over the full range with Eq. (11) extended with a linear term $E|T - T_c|$ (with $E$ being an additional adjusted parameter), resulted in values closer to 0.5. For the NI transitions of the other mixtures of 8OCB+9DBT and 9OCB+9DBT very similar results from $c_p$ fits were obtained. On the basis of the value of other critical exponents, in particular the value of the order parameter critical exponent $\beta$ **[48, 49]**, Keyes **[50]** and Anisimov *et al.* **[51, 52]** formulated arguments that tricritical values should be expected for the NI transition. However, conflicting results are obtained for the same parameters in fitting equations when deduced from measurements of different physical properties. For example, the values for $(T^* - T_{NI})$ and $(T^{**} - T_{NI})$ obtained from specific heat capacity data are consistently an order of magnitude smaller than values derived from several other physical quantities (see e.g. **[41]** and references therein). Additional theoretical and experimental work seems to be imperative for resolving these remaining inconsistencies. In particular, experiments imposing external fields might allow closer approaches to the possible tricritical point.

*4.4 Smectic A to nematic transition*

Since the beginning of the 1970s, the AN transition has been vigorously investigated experimentally and theoretically. Initially, much attention was devoted to mean-field considerations **[33-36]**, which proposed first-order (discontinuous) or second-order (continuous) transitions, depending on the coupling between the smectic and the nematic order parameters, which in turn is related to the width of the nematic temperature range. Depending on the value of the parameter $c$ in Eq. (6), one has a first-order transition for $c < 0$ and second-order one for $c > 0$. Experimentally, in the 1970s differential scanning calorimetry (DSC) was mainly used to address the issue of the order of the transition. It was generally concluded that for all the studied systems the transitions were first order. However, by the end of the 1970s it

became clear **[53-55]** that DSC was not the proper tool for this type of assessment, because it does not allow one to distinguish between true latent heats and pretransitional (fluctuations-induced) enthalpy changes **[41]**. Effectively second-order systems with very small upper limits for true latent heats were reported, as well as tricritical points located at crossover points from first-order to second-order along transition lines **[56, 57]**. Halperin, Lubensky and Ma **[37, 38]** theoretically predicted that the AN phase transition should always be (at least weakly) first order because of the coupling between the smectic order parameters and nematic director fluctuations. Nevertheless, it was not possible to address this hypothesis with appropriate experimental resolution until the late 1980s. It turned out that experimental upper limits for true latent heats for some systems, obtained by high-resolution calorimetry, were fully consistent with the analysis in terms of the theoretical prediction **[39]**.

*4.4.1 Latent heat values*

The fact that the direct result of adiabatic scanning calorimetry is a data set of enthalpy versus temperature data (see Eq. (9)) allows one to make a distinction between first-order (presence of latent heat) and second-order (absence of latent heat) transitions. In an ideal first-order transition, the presence of latent heat corresponds to a vertical step at the transition temperature in the enthalpy versus temperature curve. In practice there is always a small inclination (see **Fig. 7** for the NI transition) corresponding with a small (impurity induced) two-phase region. This is not different for the *N*-Sm*A* transition, because even minute amounts of impurities cannot be avoided. However, the large amounts of enthalpy data points and high-resolution in temperature allow one to look for linear parts and slope discontinuities in the (higher) derivatives, so as to delimit two-phase regions and determine the latent heats. Improving visibility and resolution can be substantially enhanced by subtracting a linear temperature dependent enthalpy increase (corresponding with a constant background heat capacity) from the direct experimental data. This is illustrated in **Fig. 8** for two mixtures of 9OCB+9DBT. Table 6 lists the latent heat values, being very small for several of the mixtures, for the two systems 8OCB+9DBT and 9OCB+9DBT. For pure 8OCB, the given value is the upper limit presented in **[22]**, for pure 9OCB the new result corresponds with the value of **[22]**. An overview of the latent heat date of Table 6 is depicted in **Fig. 9**.

*4.4.2 Specific heat capacity and effective critical exponents*

Second-order (continuous) phase transitions are characterized by fluctuations, which, for a properly defined order-parameter, diverge in size to infinity. This size divergence can be described by a power law, with a characteristic critical exponent that depends on the universality class of the phase transition. The limiting behavior of the specific heat capacity at a second-order transition can also be described by means of a power law of the form given in Eq. (11) of section 4.3. Normally, the different coefficients in Eq. (11) are derived from (non-linear) least-squares fitting of experimental $c_p(T)$ data. However, the fact that ASC scans result directly in enthalpy $h(T)$ data (see Eq. (9)) allows for substantial simplification. One can define the following quantity:

$$C = \frac{h - h_c}{T - T_c}, \tag{12}$$

which corresponds with the slope of the chord connecting $h(T)$ at $T$, with $h_c$ at $T_c$ It can easily be shown, that $C$ has a power law behavior of the form **[55]**:

$$C = \frac{A}{1-\alpha}|\tau|^{-\alpha} + B\,. \tag{13}$$

Both $c_p$ and $C$ have the same critical exponent, and either equation (11) or (13) can be used in fitting data to arrive at important values for the critical exponent $\alpha$ and amplitude $A$. However, by considering the difference ($C - c_p$), above or below $T_c$, the (unimportant) background term $B$ drops out, resulting in:

$$C - c_p = \frac{\alpha A}{1-\alpha}|\tau|^{-\alpha}\,. \tag{14}$$

Taking the logarithm on both sides of Eq. (6) gives:

$$\log\left(C - c_p\right) = \log\left(\frac{\alpha A}{1-\alpha}\right) - \alpha \log|\tau|\,. \tag{15}$$

As a result, one obtains a straight line with a negative slope immediately giving the critical exponent $\alpha$.

Strictly speaking, this procedure is applicable only to second-order transitions, but for weakly first-order transitions it can be used for separate analyses of the data below and above the transition. This is done by allowing $T_c$ and $h_c$ in Eq. (12) to be adjustable parameters in fitting that can be different for data below and above the transition. This is analogous to the upper stability limit of the nematic phase and the lower stability limit for the weakly first-order NI transition (see section 4.3). We have applied this approach to the present phase transition data of $c_p$ and $h$ for the different 8OCB+9DBT and 9OCB+9DBT mixtures, excluding the data in the two-phase region. In view of the smallness of the relevant latent heats, typically an order of magnitude smaller than for the *NI* transition, this approach is quite feasible.

In **Fig. 10** a comparison is made between the direct $c_p(T)$ and $C(T)$ data for the 8OCB+9DBT mixture with $x_{8OCB}$ =0.304. Obviously, the $C(T)$ are larger than the $c_p(T)$ because for the enthalpy curve the chord ($C$) between $T$ and $T_c$ is always steeper than the local slope ($c_p$) at $T$. The above described approach has been applied to all the mixtures of 8OCB+9DBT and 9OCB+9DBT. Using Eq. (15) allows one to derive from the negative slope in a double-logarithmic plot (see e.g. **Fig. 11**) of the ($C$-$c_p$) versus $|\tau|$ data to extract the (effective) critical exponent $\alpha_{eff}$. The resulting $\alpha_{eff}$ values for the different mixtures are displayed in **Fig. 12** as a function of the McMillan [24] parameter $T_{AN}/T_{NI}$, the ratio of the temperatures (in K) of the AN and NI transitions. Slightly different symbols are used for $\alpha_{eff}$ for mixtures between pure 9DBT and the concentration with the lowest AN transition temperature (henceforth referred to as low $x_{9OCB}$ regime) and between the concentration with the lowest AN transition temperature and pure 9OCB (henceforth referred to as high $x_{9OCB}$ regime). In the same figure, the $\alpha_{eff}$ values obtained by previous calorimetric and optical measurements, available in literature **[18-22, 25, 26, 29, 51, 57, 58]** have been included.

*4.4.3 Halperin-Lubensky-Ma effect*

As explained in the previous sections, Halperin *et al.* **[37, 38]** argued that the existing coupling between the nematic director fluctuations and the smectic order parameter should always lead the AN transition to be (at least weakly) first order. This coupling can be described by the addition of a cubic term in the free energy expansion, as later on formulated by Anisimov *et al.*

**[39]**. In particular, on the basis of Eq. (6) they arrived at a universal function (Eq. (8)) for the reduced entropy discontinuity, $s$, near a Landau-tricritical point. By means of this universal function, they revisited and reanalyzed all the experimental data available at that time, indicating the validity of Halperin-Lubensky-Ma hypothesis. In the following, we present a similar analysis for the 8OCB+9DBT and 9OCB+9DBT mixtures. In **Fig. 13** the reduced entropy discontinuity $s = \Delta S/R$ (R being the gas constant) is plotted as a function of the mole fraction $x$. Note that $x$ corresponds to either $x_{9DBT}$ (for 8OCB+9DBT and 9OCB+9DBT low $x_{9OCB}$ regime) or $x_{9OCB}$ (9OCB+9DBT high $x_{9OCB}$ regime). The fitting curves obtained by the universal function of Eq. (8) are also presented in this figure. The fits nicely follow the mole fraction dependence of $s$, demonstrating that our results are fully consistent with the presence of a cubic term in the free energy due to the Halperin-Lubensky-Ma effect. Landau-tricritical points are obtained at mole fractions $x^* = 0.7106$ (8OCB+9DBT), $x^* = 0.7285$ (9OCB+9DBT low $x_{9OCB}$ regime) and $x^* = 0.9722$ (9OCB+9DBT high $x_{9OCB}$ regime). Non-zero latent heat values are clearly observed at these mole fractions (and further on), suggesting that the presence of a cubic term in the free energy is indispensable to properly describe the AN transition behavior of all mixtures.

Based on the fitting parameters, the reduced entropy discontinuity $s/s^*$ is plotted as a function of $y$-$y^*$ in the upper part of **Fig. 14**. In this scaled (normalized) representation, fine agreement exists between the mixtures; the Landau lines as well as the universal function fits essentially coincide. Finally, in **Fig. 15** the normalized universal scaling is represented using a logarithmic $s/s^*$ scale. This type of representation increases the clarity in the regime of low $s/s^*$ values, reaching the experimental limits of high-resolution calorimetry for detecting latent heat. The upper limits for possible non-zero latent heat of the AN transition of pure 8CB **[17, 55]** and 8OCB **[22]** are also included in this plot. In the lower part of **Fig. 15**, in a similar semi-logarithmic plot, a comparison is made with the same fitting curve as in the upper part of the figure and $s/s^*$ data derived from optical measurements (mainly birefringence). Very good correspondence is observed with the exception of the data of **[59, 60]** in the negative ($y - y^*$) range. The data points marked by vertical bars correspond to the upper limits of entropy discontinuities that can be detected as enthalpy jumps (due to latent heat) in calorimetric measurements **[18, 22, 55]** or order parameter jumps in optical (birefringence) measurements **[25, 26]**.

## 5. Summary and conclusion

A systematic study of the phase transition behavior of several binary mixtures of liquid crystals belonging to different homologous series has been performed by means of Peltier-element-based adiabatic scanning calorimetry (pASC). Two mixture systems were chosen: the liquid crystal smectic $A_1$ compound 5-n-nonyl-2-(4'-isothiocyanatophenyl)dioxane-1.3 (9DBT) on one side, and one of the smectic $A_d$ compounds 4-n-octyloxy-4'-cyanobiphenyl (8OCB) and 4-nonyloxy-4'cyanobiphenyl (9OCB) on the other side. The temperature dependence of specific heat capacity and enthalpy has been analyzed along the nematic-isotropic (NI), smetic A-nematic (AN), smectic A-isotropic (AI) and smectic A-to-solid phase transitions. The respective phase diagrams display similar shapes. However, when mixed with 9DBT, physicochemical differences between 8OCB and 9OCB are reflected in the different thermal stability of the different phases and the eutectic point location. These precise phase diagrams

revealed strong mixing induced enhancement in the width of the nematic range with clear minima along the AN transition line for compositions, different for both systems but not far from equimolar. For the liquid crystal-to solid transitions, melting and eutectic transition heats have been obtained and the eutectic point mole fractions have been located for both systems. The NI transitions are weakly first order with latent heat values in the range usually observed for this transition in other liquid crystals. The critical behavior of the specific heat capacity at the NI transition is described by exponent values near the tricritical one of 0.5.

For the AN transitions, the specific heat capacity temperature dependence $c_p(T)$ has been analyzed using a power law for all mixtures. The resolution of pASC has allowed us to collect $c_p$ data corresponding to essentially small reduced-temperature values $|\tau|$ (down to $10^{-4}$) and derive the critical exponent values. The effective critical exponent values for the specific heat capacity of the AN transitions follow the McMillan ratio-dependence. Along the AN transition lines, strong composition dependence was observed for the latent heat. The fitting of these AN latent heat values, using the universal function of Anisimov *et al.* **[39]** (which, compared to earlier models, contains a non-zero cubic term in the free energy dependence on the order parameter), is fully consistent with the presence of the Halperin-Lubensky-Ma effect and the weakly-first-order character of the NA transition in the present mixtures of liquid crystals belonging to different homologous series.

**Declaration of competing interest**

No potential conflict of interest is reported by the authors.

**Acknowledgments**

G.C. acknowledges the financial support of the Projects CZ.02.2.69/0.0/0.0/16_027/0008465 for Mobility of Researchers under the Operational Programme Research, Development and Education and P1-0125 of the Slovenian Research Agency.

**References**

[1] P. G. de Gennes, J. Prost, The Physics of Liquid Crystals, Oxford University Press, Oxford, 1993.
[2] G. Vertogen, W.H. de Jeu, Thermotropic Liquid Crystals: Fundamentals, Springer-Verlag, Berlin, 1988.
[3] P. J. Collings, M. Hird, Introduction to Liquid crystals: Chemistry and Physics, Taylor & Francis, London, 1997.
[4] J. Thoen, H. Marynissen and W. Van Dael, Nematic-Smectic-A Tricritical Point in Alkylcyanobiphenyl Liquid Crystals, Phys. Rev. Lett. 52 (1984) 204-207. https://doi.org/10.1103/PhysRevLett.52.204
[5] C. W. Garland and G. Nounesis, Critical behavior at nematic – smectic-A phase transitions, Phys. Rev. E 49 (1994) 2964-2971. https://doi.org/10.1103/PhysRevE.49.2964
[6] Z. Kutnjak, C. W. Garland, C. G. Schatz, P. J. Collings, C. J. Booth and J. W. Goodby, Critical point for the blue-phase-III–isotropic phase transition in chiral liquid crystals, Phys. Rev. E 53 (1996) 4955-4963. https://doi.org/10.1103/PhysRevE.53.4955
[7] M. A. Anisinov, V. A. Agayan and P. J. Collings, Nature of the Blue-Phase-III–isotropic critical point: An analogy with the liquid-gas transition, Phys. Rev. E 57 (1998) 582-595. https://doi.org/10.1103/PhysRevE.57.582

[8] T. Bellini, L. Radzihovsky, J. Toner and N. A. Clark, Universality and Scaling in the Disordering of a Smectic Liquid Crystal, Science 294 (2001) 1074-1079. https://doi.org/10.1126/science.1057480

[9] G. S. Iannacchione, S. Park, C. W. Garland, R. J. Birgenaeu and R. L. Leheny, Smectic ordering in liquid-crystal–aerosil dispersions. II. Scaling analysis, Phys. Rev. E 67 (2003) 011709. https://doi.org/10.1103/PhysRevE.67.011709

[10] H. Ozbek, S. Ustunel, E. Kutlu and M. C. Çetinkaya, A simple method to determine high-accuracy refractive indices of liquid crystals and the temperature behavior of the related optical parameters via high-resolution birefringence data, J. Mol. Liq. 199 (2014) 275-286. https://doi.org/10.1016/j.molliq.2014.09.003

[11] D. Pociecha, C. A. Crawford, D. A. Paterson, J. M. D. Storey, C. T. Imrie, N. Vaupotič and E. Gorecka, Critical behavior of the optical birefringence at the nematic to twist-bend nematic phase transition, Phys. Rev. E 98 (2018) 052706. https://doi.org/10.1103/PhysRevE.98.052706

[12] V. Swaminathan, V. P. Panov, A. Panov, D. Rodriguez-Lojo, P. J. Stevenson, E. Gorecka and J. K. Vij, Design and electro-optic investigations of de Vries chiral smectic liquid crystals for exhibiting broad temperature ranges of SmA* and SmC* phases and fast electro-optic switching, J. Mater. Chem. C 8 (2020) 4859-4868. https://doi.org/10.1039/C9TC04405A

[13] E. Anesta, G. S. Iannacchione and C. W. Garland, Critical linear thermal expansion in the smectic-*A* phase near the nematic-smectic phase transition, Phys. Rev. E 70 (2004) 041703. https://doi.org/10.1103/PhysRevE.70.041703

[14] R. Dabrowski, From the discovery of the partially bilayer smectic A phase to blue phases in polar liquid crystals, Liq. Cryst. 42 (2015) 783-818, and references therein. https://doi.org/10.1080/02678292.2014.987705

[15] J. Caerels, C. Glorieux, J. Thoen, Photopyroelectric ac calorimetric study of the nematic-smectic-A phase-transition line in binary liquid crystal mixtures with injected smectic-A phases, Phys. Rev. E 65 (2002) 031704. https://doi.org/10.1103/PhysRevE.65.031704

[16] K. Denolf, B. Van Roie, C. Glorieux, J. Thoen, Effect of Nonmesogenic Impurities on the Order of the Nematic to Smectic-A Phase Transition in Liquid Crystals, Phys. Rev. Lett. 97 (2006) 107801. https://doi.org/10.1103/PhysRevLett.97.107801

[17] J. Thoen, H. Marynissen, W. Van Dael, Heat Capacity and Enthalpy Behavior Near Phase Transitions in Some Alkylcyanobiphenyls Mol. Cryst. Liq. Cryst. 97 (1983) 149-161. https://doi.org/10.1080/00268948308073147

[18] H. Marynissen, J. Thoen, W. Van Dael, Experimental Evidence for a Nematic to Smectic A Tricritical Point in Alkylcyanobiphenyl Mixtures, Mol. Cryst. Liq. Cryst. 124 (1985) 195-203. https://doi.org/10.1080/00268948508079476

[19] M. A. Anisimov, V. P. Voronov, A. O. Kulkov, V. N. Petukhov, F. Kholmurodov, High-Resolution Adiabatic Calorimetry Measurements in the Vicinity of the Liquid Crystal Phase Transitions, Mol. Cryst. Liq. Cryst. 150B (1987) 399. https://doi.org/10.1080/00268948708074812

[20] K. J. Stine, C. W. Garland, Calorimetric study of nematic to smectic-*A* tricritical behavior, Phys. Rev. A 39 (1989) 3148-3156. https://doi.org/10.1103/PhysRevA.39.3148

[21] J. Caerels, C. Glorieux, J. Thoen, Photopyroelectric ac calorimetric investigation of phase transition lines in liquid crystal mixtures, Anal. Sci. 17 (2001) s81-s84.

[22] G. Cordoyiannis, C. S. P. Tripati, C. Glorieux, J. Thoen, Order of phase transitions and tricriticality in mixtures of octyloxycyanobiphenyl and nonyloxycyanobiphenyl liquid crystals:

A high-resolution study by adiabatic scanning calorimetry, Phys. Rev. E 82 (2010) 031707. https://doi.org/10.1103/PhysRevE.82.031707

[23] M. C. Çetinkaya, S. Yildiz, H. Özbek, P. Losada-Pérez, J. Leys, J. Thoen, High-resolution birefringence investigation of octylcyanobiphenyl (8CB): An upper bound on the discontinuity at the smectic-A to nematic phase transition, Phys. Rev. E 88 (2013) 042502. https://doi.org/10.1103/PhysRevE.88.042502

[24] J. Salud, D. O. Lopez, S. Diez-Berart, M. R. de la Fuente, Tests of the tricritical point in the SmA-to-N phase transition of binary mixtures of butyloxybenzylidene octylaniline and hexyloxybenzylidene octylaniline, Liq. Cryst. 40 (2013) 293-304. https://doi.org/10.1080/02678292.2012.742580

[25] S. Yildiz, M. C. Çetinkaya, S. Üstünel, H. Özbek, J. Thoen, Test of Halperin-Lubensky-Ma crossover function at the N–Sm−A transition in liquid crystal binary mixtures via high-resolution birefringence measurements, Phys. Rev. E 93 (2016) 062706. https://doi.org/10.1103/PhysRevE.93.062706

[26] M. C. Çetinkaya, S. Üstünel, H. Özbek, S. Yildiz, J. Thoen, Convincing evidence for the Halperin-Lubensky-Ma effect at the N-SmA transition in alkyloxycyanobiphenyl binary mixtures via a high-resolution birefringence study, Eur. Phys. J. 41 (2018) 129. https://doi.org/10.1140/epje/i2018-11738-0

[27] K. Denolf, G. Cordoyiannis, C. Glorieux, J. Thoen, Effect of nonmesogenic impurities on the liquid crystalline phase transitions of octylcyanobiphenyl, Phys. Rev. E 76 (2007) 051702. https://doi.org/10.1103/PhysRevE.76.051702

[28] K. P. Sigdel, G. S. Iannacchione, Calorimetric study of the nematic to smectic-A phase transition in octylcyanobiphenyl-hexane binary mixtures, Phys. Rev. E 82 (2010) 051702. https://doi.org/10.1103/PhysRevE.82.051702

[29] C. S. P. Tripathi, P. Losada-Pérez, J. Leys, G. Cordoyiannis, C. Glorieux, J. Thoen, Evidence from adiabatic scanning calorimetry for the Halperin-Lubensky-Ma effect at the N-SmA phase transitions in mixtures of 7OCB+heptane with an injected SmA phase, Eur. Phys. J. E 35 (2012) 54. https://doi.org/10.1140/epje/i2012-12054-5

[30] K. Czupryński, R. Dabrowski, J. Baran, A. Żywociński, J. Przedmojski, A nematic gap in mixtures of smectics A1 and Ad, J. Physique 47 (1986) 1577-1585. https://doi.org/10.1051/jphys:019860047090157700

[31] J. Leys, P. Losada-Pérez, C. Glorieux, J. Thoen, The melting behaviour of water and water-sodium chloride solutions studied by high-resolution Peltier-element-based adiabatic scanning calorimetry, J. Therm. Anal. Calorim. 129 (2017) 1727-1739. https://doi.org/10.1007/s10973-017-6330-4

[32] J. Thoen, Thermal investigations of phase transitions in thermotropic liquid crystals, Int. J. Mod. Phys. B **9** (1995) 2157-2218. https://doi.org/10.1142/S0217979295000860

[33] K. Kobayashi, On the theory of translational and orientational melting with application to liquid crystals, Phys. Lett. A 31 (1970) 125-126. https://doi.org/10.1016/0375-9601(70)90186-6

[34] W.L. McMillan, Simple Molecular Model for the Smectic A Phase of Liquid Crystals, Phys. Rev. A 4 (1973) 1238-1246. https://doi.org/10.1103/PhysRevA.4.1238

[35] P. G. de Gennes, An analogy between superconductors and smectics A, Solid State Commun. 10 (1972) 753-756. https://doi.org/10.1016/0038-1098(72)90186-X

[36] P. G. de Gennes, Some Remarks on the Polymorphism of Smectics, Mol. Cryst. Liq; Cryst. 21 (1973) 49-76. https://doi.org/10.1080/15421407308083313

[37] B. I Halperin, T. C. Lubensky, K. Ma, First-Order Phase Transitions in Superconductors and Smectic-A Liquid Crystals, Phys. Rev. Lett. 32 (1974) 292-295. https://doi.org/10.1103/PhysRevLett.32.292
[38] B. I Halperin, T. C. Lubensky, On the analogy between smectic a liquid crystals and superconductors, Solid State Commun. 14 (1974) 997-1001. https://doi.org/10.1016/0038-1098(74)90411-6
[39] M. A. Anisimov, P.E. Cladis, E. E. Gorodetskii, V. E . Podneks, V. G. Taratuta, W. van Saarloos, V. P. Voronov, Experimental test of a fluctuation-induced first-order phase transition: The nematic–smectic-*A* transition, Phys. Rev. A 41 (1990) 6749-6762. https://doi.org/10.1103/PhysRevA.41.6749
[40] J. Thoen, E. Bloemen, H. Marynissen, W. Van Dael, Proceedings of the 8th Symposium on Thermophysical Properties, Nat. Bur. Standards, Maryland, USA, 1981, Ed. J. V. Sengers, Am. Soc. Mechan. Eng., New York (1982) p. 422-428.
[41] J. Thoen, in: Phase Transitions in Liquid Crystals, NATO ASI Ser. B, Eds. S. Martellucci and A. N. Chester, Plenum, New York (1992) pp 155-174.
[42] J. Thoen, in: Heat Capacities: Liquids, Solutions and Vapours, Ed. E. Wilhelm, T. M. Letcher, The Royal Soc. Chem., London (2010) Chap. 13.
[43] J. Thoen, J. Leys, C. Glorieux, European Patent EP 2 91328 B1 (Sept 02, 2015), US patent US 9.310.263 B2 (April 12, 2016).
[44] J. Leys, P. Losada-Pérez, C. Glorieux, J, Thoen, Application of a novel type of adiabatic scanning calorimeter for high-resolution thermal data near the melting point of gallium, J. Therm. Anal. Calorim. 117 (2014) 173-187. https://doi.org/10.1007/s10973-014-3654-1
[45] J. Leys, P. Losada-Pérez, E. Slenders, C. Glorieux, J. Thoen, Investigation of the melting behavior of the reference materials biphenyl and phenyl salicylate by a new type adiabatic scanning calorimeter, Thermochim. Acta, 582 (2014) 68-76. https://doi.org/10.1016/j.tca.2014.02.023
[46] J. Leys, C. Glorieux, J. Thoen, MRS Advances, Temperature Dependence of Enthalpy and Heat Capacity of Alkanes and Related Phase Change Materials (PCMs) with a Peltier-element-based Adiabatic Scanning Calorimeter, MRS Advances 1 (2016) 3835-3940. https://doi.org/10.1557/adv.2016.298
[47] J. Thoen, in: Enthalpy and Internal Energy: Liquids, Solutions and Vapours, Eds. E. Wilhelm, T. M. Letcher, The Royal Soc. Chem., London (2018) Chap. 3.
[48] I. Chirtoc, M. Chirtoc, C. Glorieux, J. Thoen, Determination of the order parameter and its critical exponent for nCB (n=5-8) liquid crystals from refractive index data, Liq. Cryst. 31 (2004) 229-240. https://doi.org/10.1080/02678290310001642540
[49] S. Yildiz, H. Özbek, C Glorieux, J. Thoen, Critical behaviour at the isotropic-nematic and nematic-smectic A phase transitions of 4-butyloxyphenyl 4 '-decyloxybenzoate liquid crystal from refractive index, Liq. Cryst. 34 (2007) 611. https://doi.org/10.1080/02678290701297974
[50] P. Keyes, Tricritical behavior at the isotropic-nematic transition, Phys. Lett. A 30 (1978) 132-134. https://doi.org/10.1016/0375-9601(78)90043-9
[51] M. A. Anisimov, V. M. Zaprudskii, V. M. Mamnitskii, E. L. Sorkin, Tricritical Behavior of Nematic Crystals Near the Transition to an Isotropic Liquid, JETP Lett. 30 (1979) 491-494.
[52] M. A. Anisimov, E. E. Gorodekskii V. M. Zaprudskii, Phase transitions with coupled order parameters, Sov. Phys. Usp. 24 (1981) 57-75. http://dx.doi.org/10.1070/PU1981v024n01ABEH004612

[53] G. B. Kasting, K. J. Lushington, C. W. Garland, Critical heat capacity near the nematic—smectic-A transition in octyloxycyanobiphenyl in the range 1-2000 bar, Phys. Rev. B, 22 (1980) 321-331. https://doi.org/10.1103/PhysRevB.22.321

[54] G. B. Kasting, C. W. Garland, K. J. Lushington, Critical heat capacity of octylcyanobiphenyl (8CB) near the nematic-smectic A transition, J. Phys. (Paris), 41 (1980) 879-884. https://doi.org/10.1051/jphys:01980004108087900

[55] J. Thoen, H. Marynissen, W. Van Dael, Temperature dependence of the enthalpy and the heat capacity of the liquid-crystal octylcyanobiphenyl (8CB), Phys. Rev. A, 26 (1982) 2886-2905. https://doi.org/10.1103/PhysRevA.26.2886

[56] B. Ocko, R. J. Birgeneau, J. D. Litster, Critical and Tricritical Behavior at the Nematic to Smectic-A Transition, M. E. Neubert, Phys. Rev. Lett. 52 (1984) 208-211. https://doi.org/10.1103/PhysRevLett.52.208

[57] D. Brisbin, R. DeHoff, T. E. Lockhart and D. L. Johnson, Specific Heat near the Nematic-Smectic-A Tricritical Point, Phys. Rev. Lett. 42 (1979) 1171-1174. https://doi.org/10.1103/PhysRevLett.43.1171

[58] F. Mercuri, M. Marinelli, U. Zammit, S. Foglietta and F. Scudieri, Photopyroelectric method Determination of the thermal parameters of liquid crystals and antiferromagnetic materials close to the phase transitions, J. Therm. Anal. 47 (1996) 87-92. https://doi.org/10.1007/bf01982688

[59] A. Yethiraj and J. Bechhoefer, Two Experimental Tests of the Halperin-Lubensky-Ma Effect at the Nematic–Smectic- A Phase Transition, Phys. Rev. Lett. 84 (2000) 3642-3645. https://doi.org/10.1103/PhysRevLett.84.3642

[60] A. Yethiraj, R. Mukhopadhyay and J. Bechhoefer, Two experimental tests of a fluctuation-induced first-order phase transition: Intensity fluctuation microscopy at the nematic-smectic-A transition, Phys. Rev.E. 65 (2002) 021702. https://doi.org/10.1103/PhysRevE.65.021702

**FIGURE CAPTIONS**

**Fig. 1** (Color online) Schematic representation of the inner part of a pASC. The sample cell is placed in good thermal contact on the top of the platform with the heater and T-sensor (e.g. thermistor or platinum resistor). The Peltier element acts as a temperature difference meter and is used to control the temperature difference between sample and adiabatic shield with a coil heater on its wall. During a heating run, the difference is kept at zero. A constant power is applied to the sample via the platform heater and the sample temperature is measured with the T-sensor.

**Fig. 2** (Color online) Transition temperatures for the different mixtures of nOCB+9DBT as a function of the mole fraction of nOCB (n = 8, 9) in the mixture. The symbols I, N and SmA denote the isotropic, nematic and smectic A phases. In the part (α) of the phase diagram precipitated solid 9DBT coexists with a liquid solution of 8OCB (or 9OCB) and 9DBT with increasing concentration of 8OCB (or 9OCB) with decreasing temperature. In part (β), one has the inverse situation with solid 8OCB (or 9OCB) precipitated in the liquid solution. In the (γ) part, separated solid 9DBT and 8OCB (or 9OCB) are present. The stars indicate direct AI transition temperatures.

**Fig. 3** Specific heat capacity and specific enthalpy results for selected 8OCB+9DBT mixtures. EU indicates the eutectic transition, M the melting, AN the smectic A-nematic and NI the nematic-isotropic transition. All mixtures exhibit in the low temperature range a mixed solid phase, a coexistence range of solid 9DBT and a solvent range with changing concentrations (see section 4.2). For $x_{8OCB} = 0.111$ the smectic A phase has a direct transition to the isotropic phase. In the two other cases, there is an intermediate nematic phase with a very weak AN transition anomaly. The inset in the top right figure gives a detailed view of the AN transition.

**Fig. 4** (Color online) Overview of the enthalpy changes over the melting and eutectic transitions for the 8OCB+9DBT and 9OCB+9DBT mixtures. Open circles are for the eutectic transition and open triangles are for the melting process. Open squares are the sum of both eutectic and melting.

**Fig. 5** (Color online) Overview of the obtained enthalpy values for a set of mole fractions of 8OCB of the system 8OCB+9DBT, showing the important features with increasing mole fraction of 8OCB: $x_{8OCB} = 0.000$; $x_{8OCB} = 0.111$; $x_{8OCB} = 0.213$; $x_{8OCB} = 0.370$; $x_{8OCB} = 0.619$. The eutectic transition temperature is constant at 41.7 °C and the melting temperature decreases with increasing $x_{8OCB}$, while the eutectic transition enthalpy increases at the expense of the melting enthalpy.

**Fig. 6** Latent heat ($L$) values for the transitions from the nematic or smectic A phase to the isotropic phase. Solid circles are for 8OCB+9DBT mixtures and open circles are for 9OCB+9DBT mixtures. The solid square and star symbols indicate the observed direct AI transitions for one 8OCB+9DBT mixture ($x_{8OCB} = 0.111$) and for pure 9DBT.

**Fig. 7** Pretransitional specific heat capacity and specific enthalpy in the N and I phases for the 8OCB+9DBT mixture with a mole fraction $x_{8OCB} = 0.914$. The two dashed vertical lines delimit the two-phase region of the transition. The enthalpy exhibits a clear step marking the (weakly) first-order character of the NI transition. In the enthalpy plot, for display reasons, a linear temperature-dependent background, $2.4(T - T_{ref})$, with $T_{ref}$ an arbitrary reference temperature, has been subtracted from the raw enthalpy data.

**Fig. 8** (Color online) Temperature dependence of the enthalpy in a 300 mK temperature range around the AN transition for two mixtures of 9OCB+9DBT. The dark red (upper) data are for $x_{9OCB} = 0.861$ and the dark yellow (lower) data for $x_{9OCB}=0.527$. Linear temperature-dependent backgrounds have been subtracted for display reasons. The dashed lines denote the first-order region in both cases.

**Fig. 9** Latent heat ($L$) results for 8OCB or 9OCB mixtures with 9DBT. Filled circles are for 8OCB+9DBT and open circles for 9OCB+9DBT. For display reasons the large value of 1.4 J/g for $x_{9OCB}=0.221$ (see Table 6) has been omitted.

**Fig. 10** (Color online) Comparison between the direct specific heat capacity $c_p$ (lower curve) and the quantity $C$ (upper curve) defined in Eq. (12) for the 8OCB+9DBT mixture with $x_{8OCB} = 0.304$.

**Fig. 11** (Color online) Double logarithmic plot of the ($C$-$c_p$) data near the AN transition in the in the smectic A phase (blue solid circles) and the nematic phase (red open circles) for four mixtures of 8OCB+9DBT with mole fractions of 8OCB increasing from top to bottom: $x_{8OCB} = 0.304$; $x_{8OCB} = 0.370$; $x_{8OCB} = 0.473$; $x_{8OCB} = 0.702$.

**Fig. 12** (Color online) The effective critical exponent ($\alpha_{eff}$) versus McMillan ratio ($T_{NI}/T_{AN}$) for the results of the present work and previous high-resolution calorimetric measurements (unless stated differently) reported in literature. Red-colored symbols: 8OCB+9DBT (solid stars); low $x_{9OCB}$ regime of 9OCB+9DBT; (open stars); high $x_{9OCB}$ regime of 9OCB+9DBT (open stars dot center). Black and white symbols: 7AB/8AB (plus signs) **[21]**; $\overline{n}$S5 (solid rhombs) **[57, 58]**; $\overline{6}$O $\overline{8}/\overline{6}$O$\overline{10}$, $\overline{6}$O$\overline{10}/\overline{6}$O$\overline{12}$ (open squares) **[19, 51]**; 4.O8/6.O8 (open rhombs) **[20]**; 8OCB/9OCB (open up triangles) **[22]**; 8OCB/9OCB optical measurements (solid circles) **[26]**; 7OCB/Heptane (crosses) **[29]**; 8CB/10CB (open inverted triangles) **[18];** 8CB/10CB optical measurements (open circles) **[25]**. The dashed and dotted lines denote the tricritical ($\alpha_{eff} = 0.5$) and the three-dimensional XY ($\alpha_{eff} = -0.007$) values of the effective critical exponent.

**Fig. 13** (Color online) The reduced entropy discontinuity ($s$) versus mixture concentration ($x$) for all mixtures of the present work: low $x_{9OCB}$ regime of 9OCB+9DBT (red open circles); high $x_{9OCB}$ regime of 9OCB+9DBT (green stars); 8OCB+9DBT (solid blue circles). The solid lines are fits using the scaling function of Eq. (8), whereas the dashed lines correspond to the Landau theory without a cubic term in the free energy, as in Eq. (5). For display reasons the two highest points of the 9OCB+9DBT low $x_{9OCB}$ regime have been left out of the plot.

**Fig. 14** (Color online) Normalized universal scaling graphical representation of Eq. (8) for all mixtures of the present work: low $x_{9OCB}$ regime of 9OCB+9DBT (red open circles); high $x_{9OCB}$ regime of 9OCB+9DBT (green stars); 8OCB+9DBT (solid blue circles). The solid lines of scaled fits and the dashed Landau lines essentially coincide.

**Fig. 15** (Color online) A normalized universal scaling representation of Eq. (8) with a logarithmic scale along the $s/s^*$ axis is depicted here, separately for calorimetric results (upper part) and for optical data (lower part). The colored data points correspond to the present work: 8OCB+9DBT (red solid stars); low $x_{9OCB}$ regime of 9OCB+9DBT (red open stars); high $x_{9OCB}$ regime of 9OCB+9DBT (red open stars dot center). The black and white symbols correspond to previous data in the literature. In the upper (calorimetric) part: $\overline{6}$O$\overline{8}/\overline{6}$O$\overline{10}$, $\overline{6}$O$\overline{10}/\overline{6}$O$\overline{12}$ (open squares) **[19, 51]**; 8CB/10CB (open inverted triangles) **[18]**; 9CB/10CB (open rhombs)

**[18];** 8OCB/9OCB (open up triangles) **[22]**; 7OCB/Heptane (crosses) **[29]**. In the lower (optical) part of the figure: 8OCB/9OCB (solid circles) **[26]**; 8CB/10CB (open circles) **[25]**; 8CB/10CB (stars) **[59, 60]**. In both parts, the solid blue line is the fit of previous data with Eq. (8), the dashed blue line defines the Landau tricritical point and bars denote the upper limits of entropy discontinuites when approaching the experimental detection limits.

**TABLES**

**Table 1.** Transition temperatures of 8OCB+9DBT mixtures.

| $x_{8OCB}$ | $T_{eutectic}$ (°C) | $T_{melt}$ (°C) | $T_{AN}$ (°C) | $T_{NI}$ (°C) | $T_{AI}$ (°C) |
|---|---|---|---|---|---|
| 0.000 | | 56.7 | | | 80.70 |
| 0.111 | 41.7 | 54.0 | | | 76.10 |
| 0.213 | 41.5 | 51.5 | 71.90 | 73.00 | |
| 0.304 | 41.7 | 50.0 | 67.50 | 72.02 | |
| 0.370 | 41.7 | 49.0 | 64.30 | 71.70 | |
| 0.473 | 41.6 | 46.8 | 60.23 | 71.49 | |
| 0.538 | 41.8 | 44.1 | 58.86 | 72.24 | |
| 0.620 | 41.8 | 42.8 | 57.48 | 73.20 | |
| 0.702 | 41.7 | 46.5 | 57.51 | 74.20 | |
| 0.732 | 41.9 | 48.0 | 57.80 | 74.90 | |
| 0.798 | 41.8 | 49.5 | 59.22 | 75.82 | |
| 0.914 | 41.8 | 52.6 | 63.25 | 78.25 | |
| 1.000 | | 55.0 | 66.90 | 80.05 | |

**Table 2.** Transition temperatures of 9OCB+9DBT mixtures.

| $x_{9OCB}$ | $T_{eutectic}$ (°C) | $T_{melt}$ (°C) | $T_{AN}$ (°C) | $T_{NI}$ (°C) | $T_{AI}$ (°C) |
|---|---|---|---|---|---|
| 0.000 | | 56.7 | | | 80.70 |
| 0.221 | 47.3 | 53.0 | 71.61 | 72.65 | |
| 0.245 | 47.0 | 51.7 | 69.92 | 71.95 | |
| 0.262 | 46.9 | 51.2 | 69.21 | 71.75 | |
| 0.305 | 47.0 | 49.7 | 67.61 | 71.36 | |
| 0.326 | 46.9 | 49.6 | 66.63 | 71.21 | |
| 0.362 | 47.1 | 49.3 | 65.66 | 71.26 | |
| 0.392 | 46.9 | 48.5 | 64.73 | 71.01 | |
| 0.444 | 47.2 | 48.2 | 63.70 | 71.20 | |
| 0.484 | 47.3 | 49.2 | 63.35 | 71.30 | |
| 0.527 | 47.0 | 51.4 | 63.17 | 71.60 | |
| 0.620 | 46.8 | 54.9 | 63.98 | 72.33 | |
| 0.717 | 46.9 | 57.4 | 66.57 | 73.87 | |
| 0.785 | 46.7 | 59.0 | 68.75 | 74.95 | |
| 0.861 | 46.7 | 61.6 | 72.00 | 76.80 | |
| 0.939 | 46.6 | 63.4 | 75.18 | 78.50 | |
| 1.000 | | 65.25 | 78.13 | 80.27 | |

**Table 3.** Transition heats for the melting and eutectic transitions of 8OCB+9DBT mixtures.

| $x_{8OCB}$ | $\Delta h_{eutectic}$ (J/g) | $\Delta h_{melt}$ (J/g) | $\Delta h_{tot}$ (J/g) |
|---|---|---|---|
| 0.000 | 0.0 | 123.0 | 123.0 |
| 0.111 | 16.9 | 101.4 | 118.3 |
| 0.213 | 36.9 | 86.2 | 123.0 |
| 0.305 | 54.5 | 65.5 | 120.0 |
| 0.370 | 67.5 | 54.0 | 121.5 |
| 0.473 | 79.1 | 37.7 | 116.8 |
| 0.538 | 99.4 | 18.1 | 117.5 |
| 0.620 | 102.0 | 8.5 | 110.5 |
| 0.702 | 82.9 | 32.8 | 115.7 |
| 0.732 | 70.0 | 44.3 | 114.3 |
| 0.798 | 54.0 | 63.6 | 117.6 |
| 0.914 | 26.0 | 98.0 | 124.0 |
| 1.000 | 0.0 | 120.0 | 120.0 |

**Table 4.** Transition heats for the melting and eutectic transitions of 9OCB+9DBT mixtures.

| $x_{9OCB}$ | $\Delta h_{eutectic}$ (J/g) | $\Delta h_{melt}$ (J/g) | $\Delta h_{tot}$ (J/g) |
|---|---|---|---|
| 0.000 | 0.0 | 123.0 | 123.0 |
| 0.221 | 53.0 | 68.4 | 121.4 |
| 0.245 | 63.3 | 59.6 | 122.9 |
| 0.262 | 68.7 | 54.2 | 122.9 |
| 0.277 | 68.7 | 54.2 | 122.9 |
| 0.305 | 78.2 | 44.3 | 122.5 |
| 0.326 | 84.9 | 36.1 | 121.0 |
| 0.362 | 96.4 | 23.5 | 119.9 |
| 0.392 | 106.3 | 13.5 | 119.8 |
| 0.444 | 113.0 | 5.3 | 118.3 |
| 0.484 | 107 | 15.4 | 122.4 |
| 0.527 | 98.7 | 26.5 | 125.2 |
| 0.620 | 75.2 | 48.0 | 123.2 |
| 0.717 | 57.5 | 61.0 | 118.5 |
| 0.785 | 40.6 | 76.1 | 116.7 |
| 0.861 | 25.9 | 94.2 | 120.1 |
| 0.939 | 10.6 | 109.0 | 119.6 |
| 1.000 | 0.0 | 120.2 | 120.2 |

**Table 5.** Latent heats for the NI or AI transitions that occur in different mixtures of 8OCB+9DBT and 9OCB+9DBT

| 8OCB+9DBT | | | 9OCB+9DBT | |
|---|---|---|---|---|
| $x_{8OCB}$ | $L_{NI}$ (J/g) | $L_{AI}$ (J/g) | $x_{9OCB}$ | $L_{NI}$ (J/g) |
| 0.000 | | 11.60 | 0.000 | |
| 0.111 | | 9.94 | 0.221 | 2.60 |
| 0.213 | 3.12 | | 0.245 | 2.50 |
| 0.304 | 2.30 | | 0.262 | 2.44 |
| 0.370 | 2.06 | | 0.305 | 2.13 |
| 0.473 | 1.88 | | 0.326 | 2.02 |
| 0.538 | 1.84 | | 0.362 | 2.00 |
| 0.620 | 1.58 | | 0.392 | 1.88 |
| 0.702 | 1.56 | | 0.444 | 1.69 |
| 0.732 | 1.48 | | 0.484 | 1.69 |
| 0.798 | 1.52 | | 0.527 | 1.69 |
| 0.914 | 1.53 | | 0.620 | 1.60 |
| 1.000 | 1.55 | | 0.717 | 1.63 |
| | | | 0.785 | 1.67 |
| | | | 0.861 | 1.91 |
| | | | 0.939 | 2.10 |
| | | | 1.000 | 2.40 |

**Table 6.** Latent heats and the effective critical exponent $\alpha_{eff}$ for the AN transition for the different mixtures of 8OCB+9DBT and 9OCB+9DBT. The dashed line separates the two sides of 9OCB+9DBT, referred to as the low $x_{9OCB}$ regime (between pure 9DBT and the concentration with the lowest AN transition temperature) and the high $x_{9OCB}$ regime (between the concentration with the lowest AN transition temperature and pure 90CB) in the HLM fits.

| 8OCB+9DBT | | | | 9OCB+9DBT | | | |
|---|---|---|---|---|---|---|---|
| $x_{8OCB}$ | $L_{NA}$ (J/g) | $T_{NA}/T_{NI}$ | $a_{eff}$ | $x_{9OCB}$ | $L_{NA}$ (J/g) | $T_{NA}/T_{NI}$ | $a_{eff}$ |
| 0.0000 | | | | 0.000 | | | |
| 0.111 | | | | 0.221 | 1.300 | 0.996704 | |
| 0.213 | 0.4350 | 0.996822 | | 0.245 | 0.950 | 0.994118 | |
| 0.304 | 0.2000 | 0.986905 | 0.43 | 0.262 | 0.630 | 0.992636 | 0.54 |
| 0.370 | 0.0750 | 0.978541 | 0.30 | 0.305 | 0.220 | 0.989115 | 0.48 |
| 0.473 | 0.0250 | 0.967338 | 0.24 | 0.326 | 0.080 | 0.986700 | 0.43 |
| 0.538 | 0.0160 | 0.961261 | 0.18 | 0.362 | 0.032 | 0.983740 | 0.38 |
| 0.620 | 0.0052 | 0.954612 | 0.16 | 0.392 | 0.027 | 0.981753 | 0.35 |
| 0.702 | 0.0038 | 0.95195 | 0.17 | 0.444 | 0.013 | 0.978220 | 0.31 |
| 0.732 | 0.0030 | 0.950869 | 0.14 | 0.484 | 0.019 | 0.976920 | 0.29 |
| 0.798 | 0.0038 | 0.952431 | 0.14 | 0.527 | 0.015 | 0.975547 | 0.29 |
| 0.914 | 0.0030 | 0.957314 | 0.16 | 0.620 | 0.015 | 0.975831 | 0.27 |
| 1.000 | 0.0018 | 0.962769 | 0.20 | 0.717 | 0.024 | 0.978964 | 0.27 |
| | | | | 0.785 | 0.036 | 0.982189 | 0.31 |
| | | | | 0.861 | 0.088 | 0.986284 | 0.36 |
| | | | | 0.939 | 0.270 | 0.990559 | 0.43 |
| | | | | 1.000 | 0.460 | 0.993945 | 0.46 |

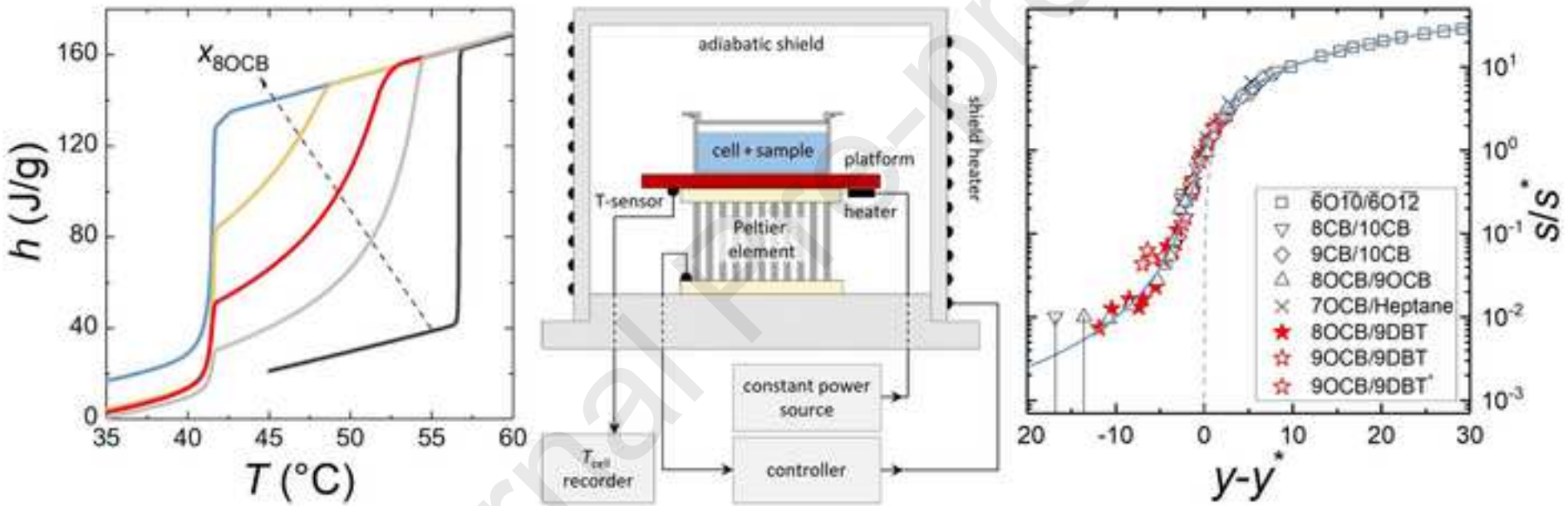

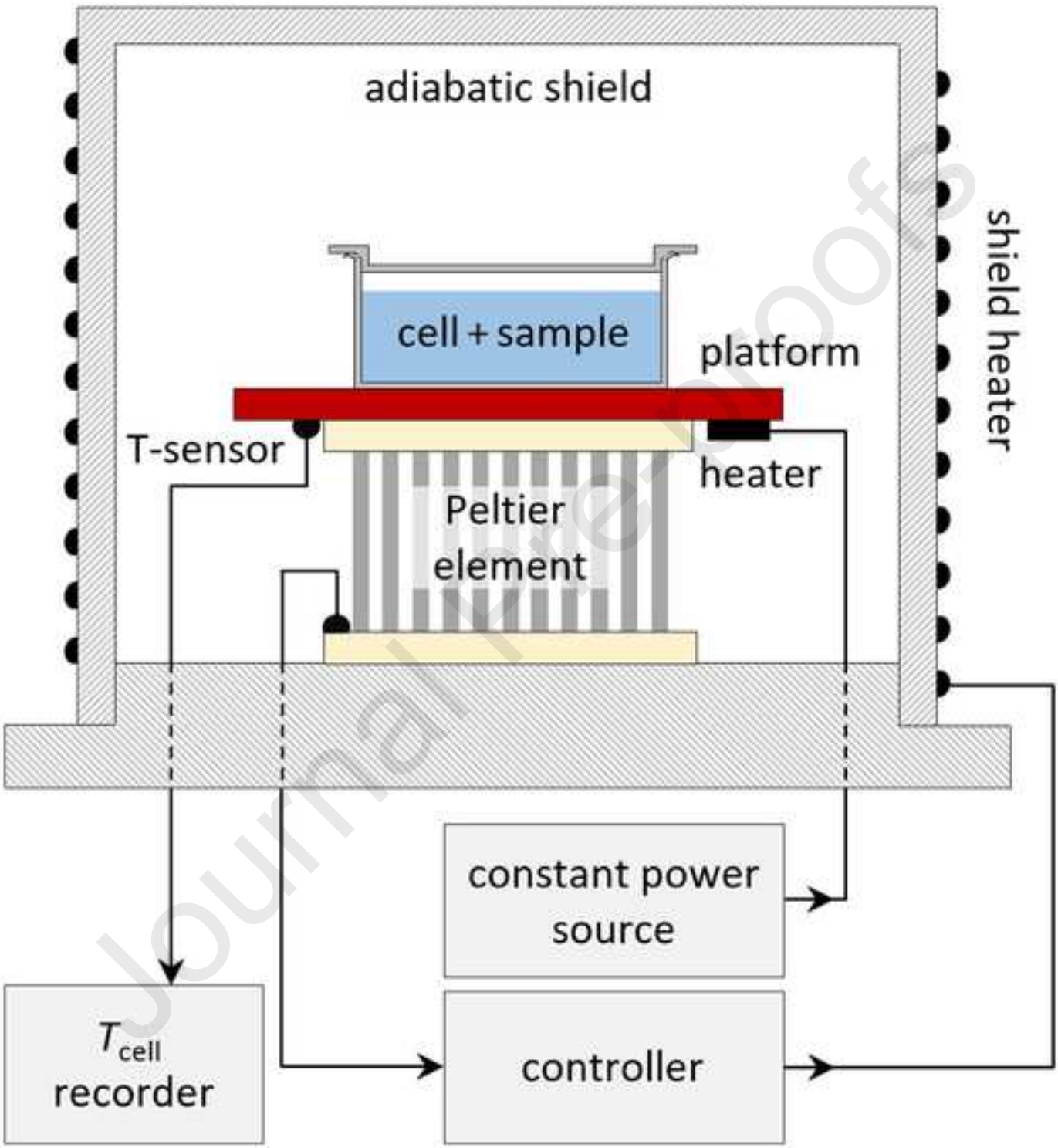

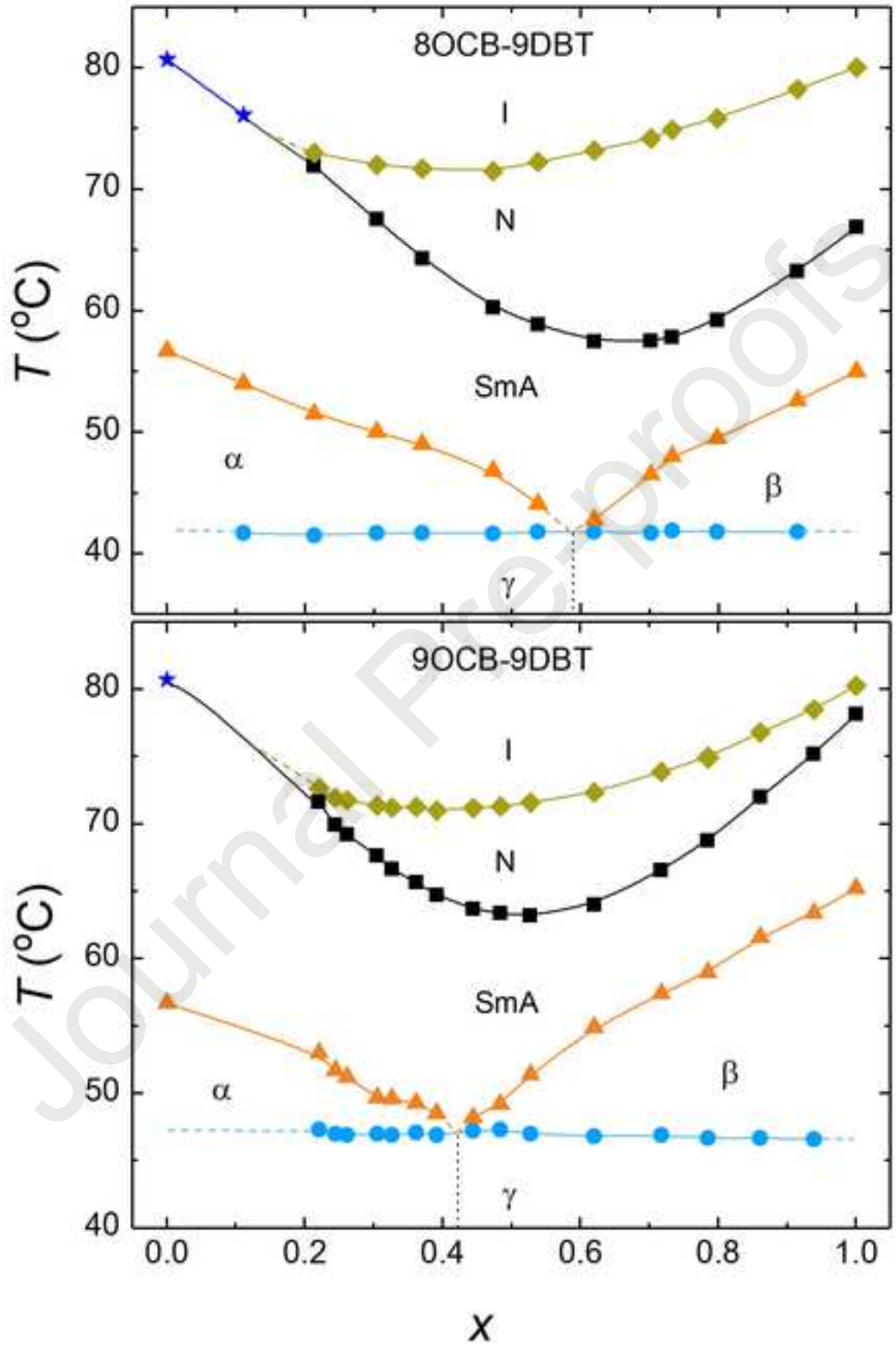

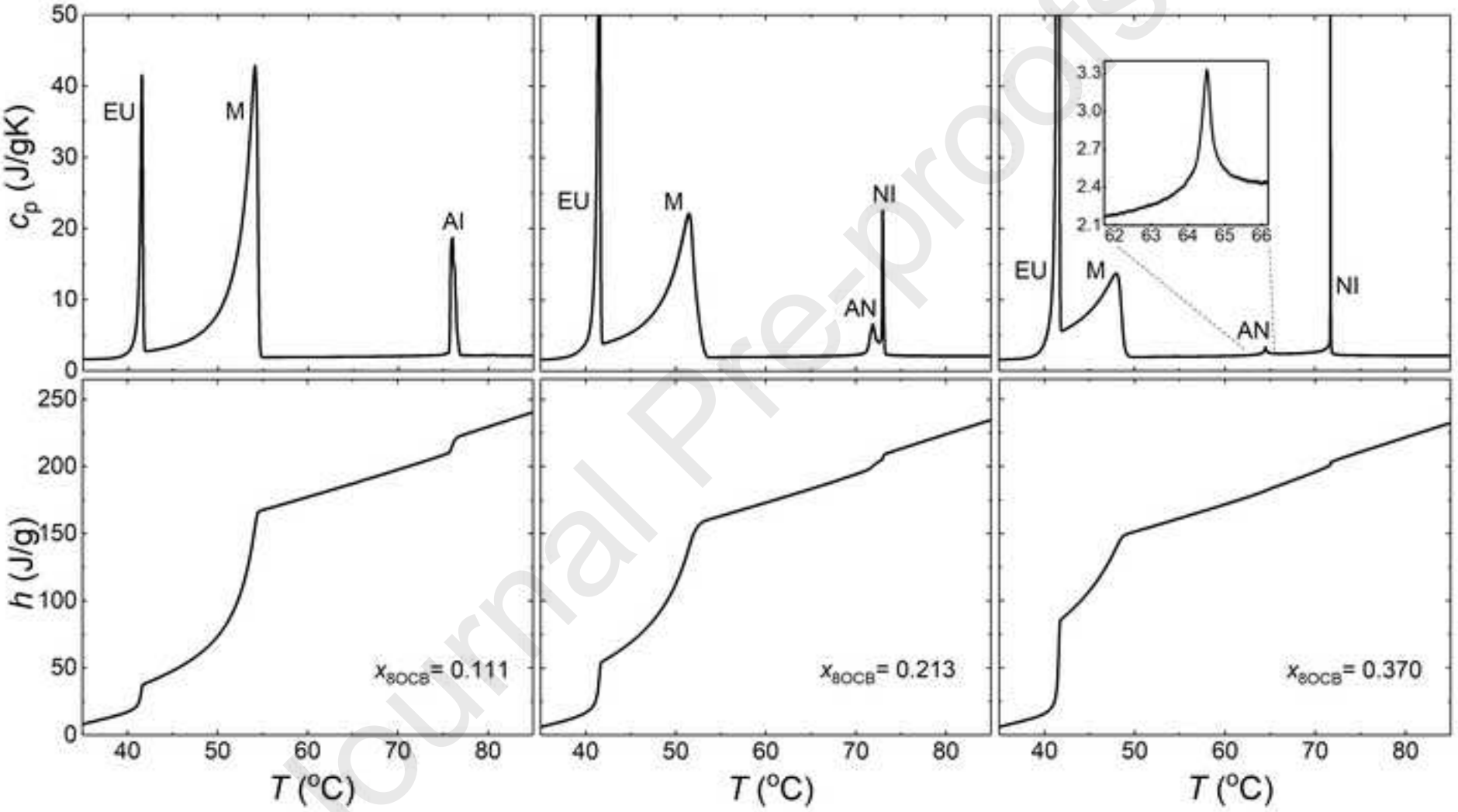

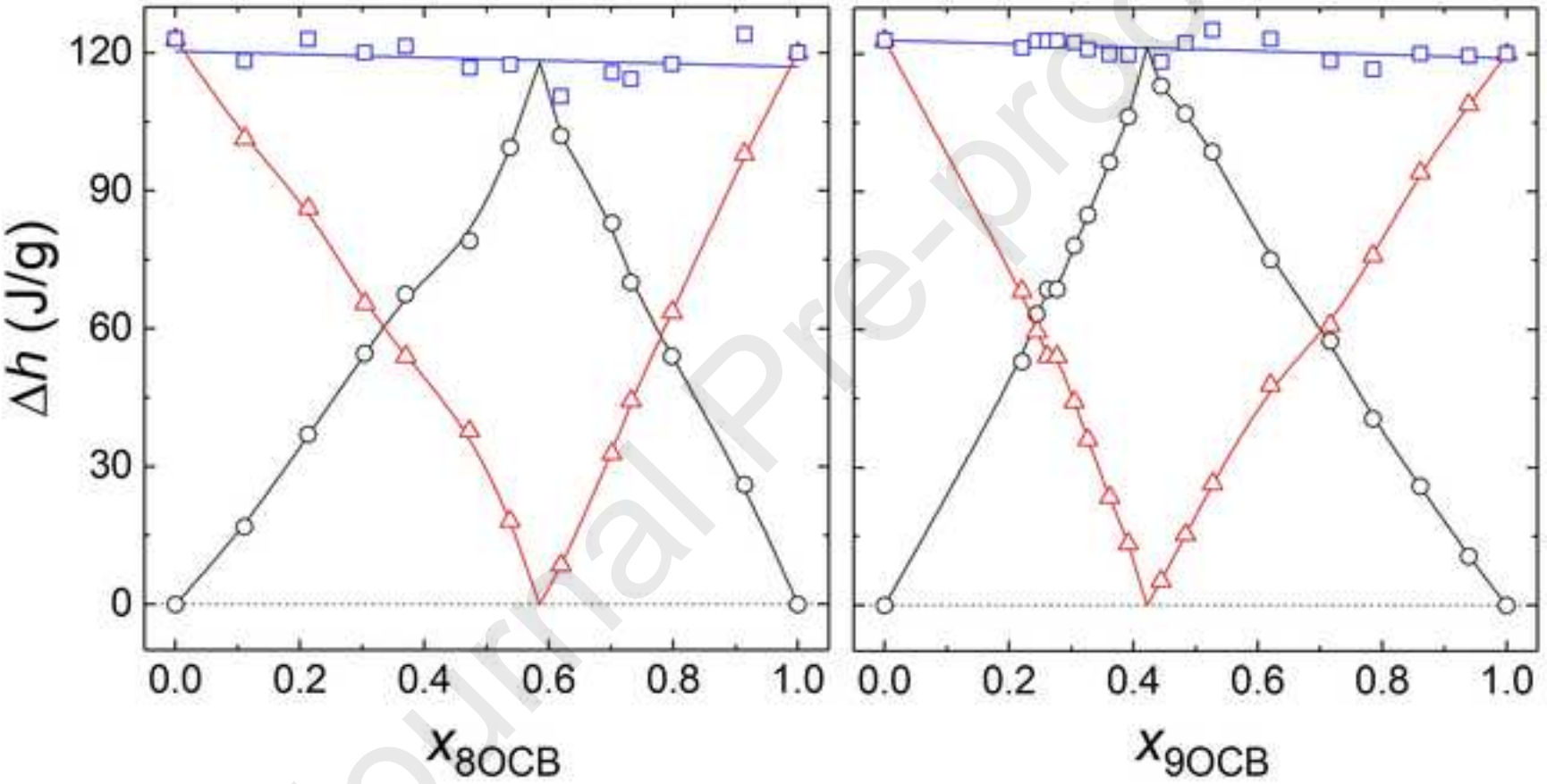

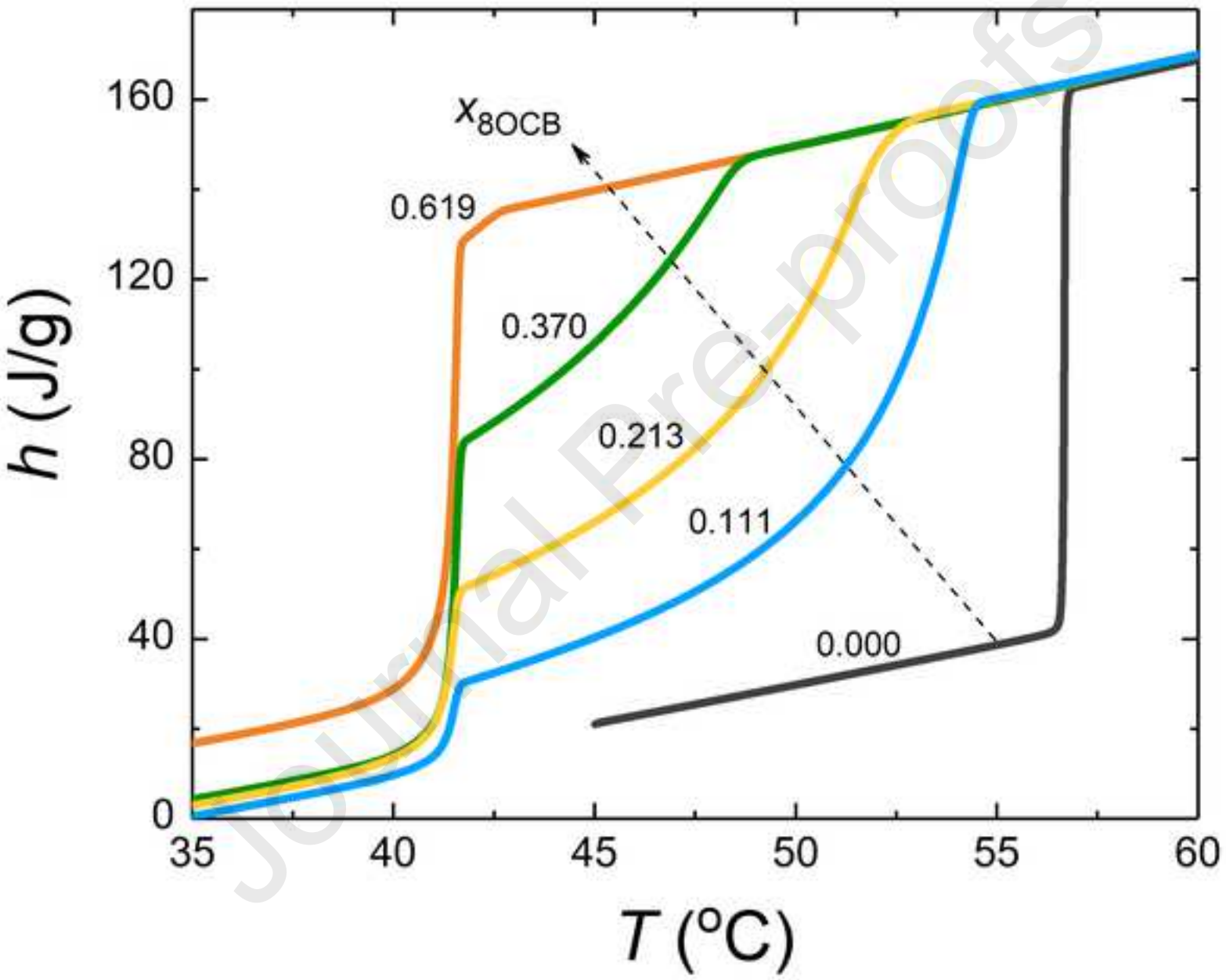

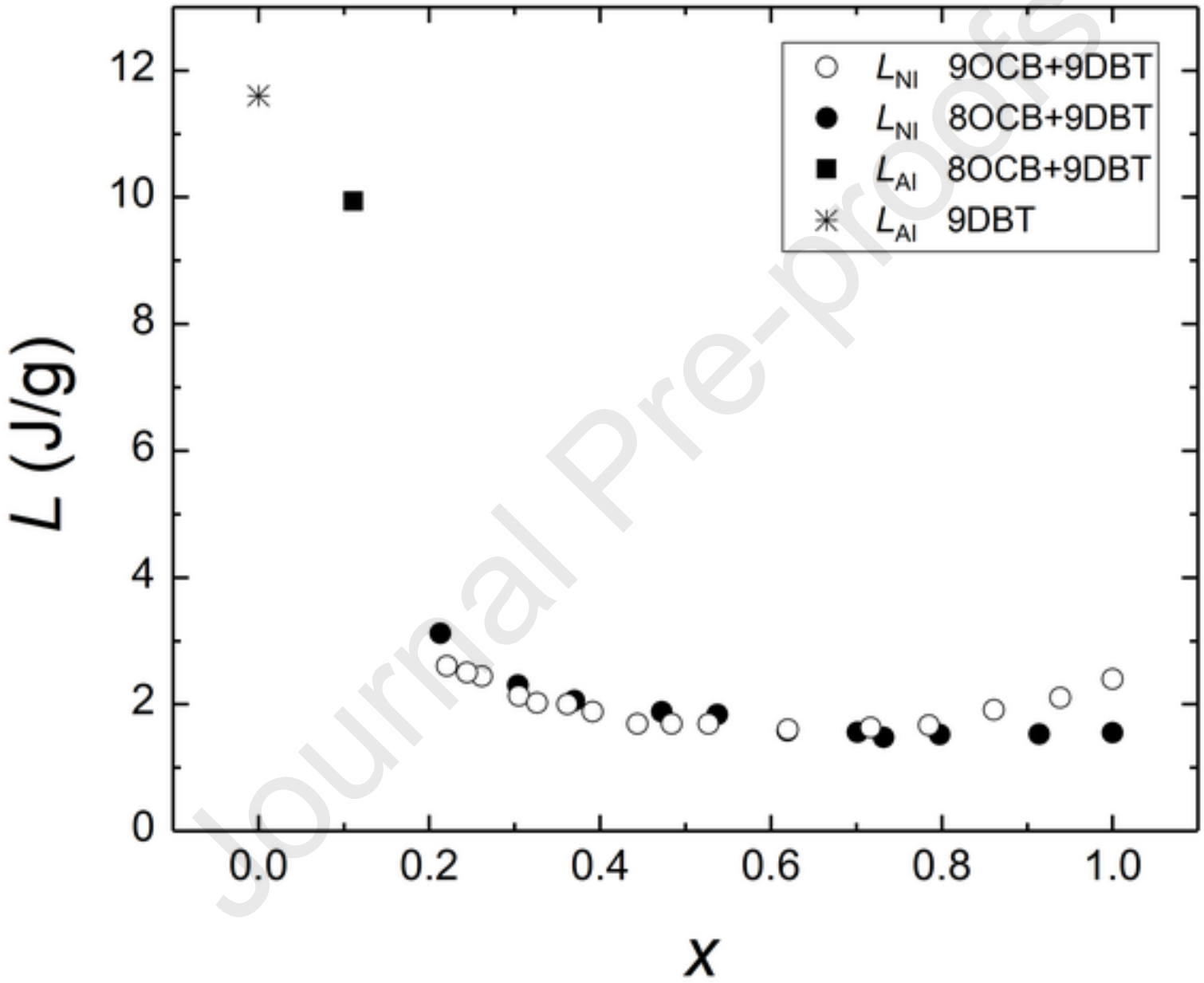

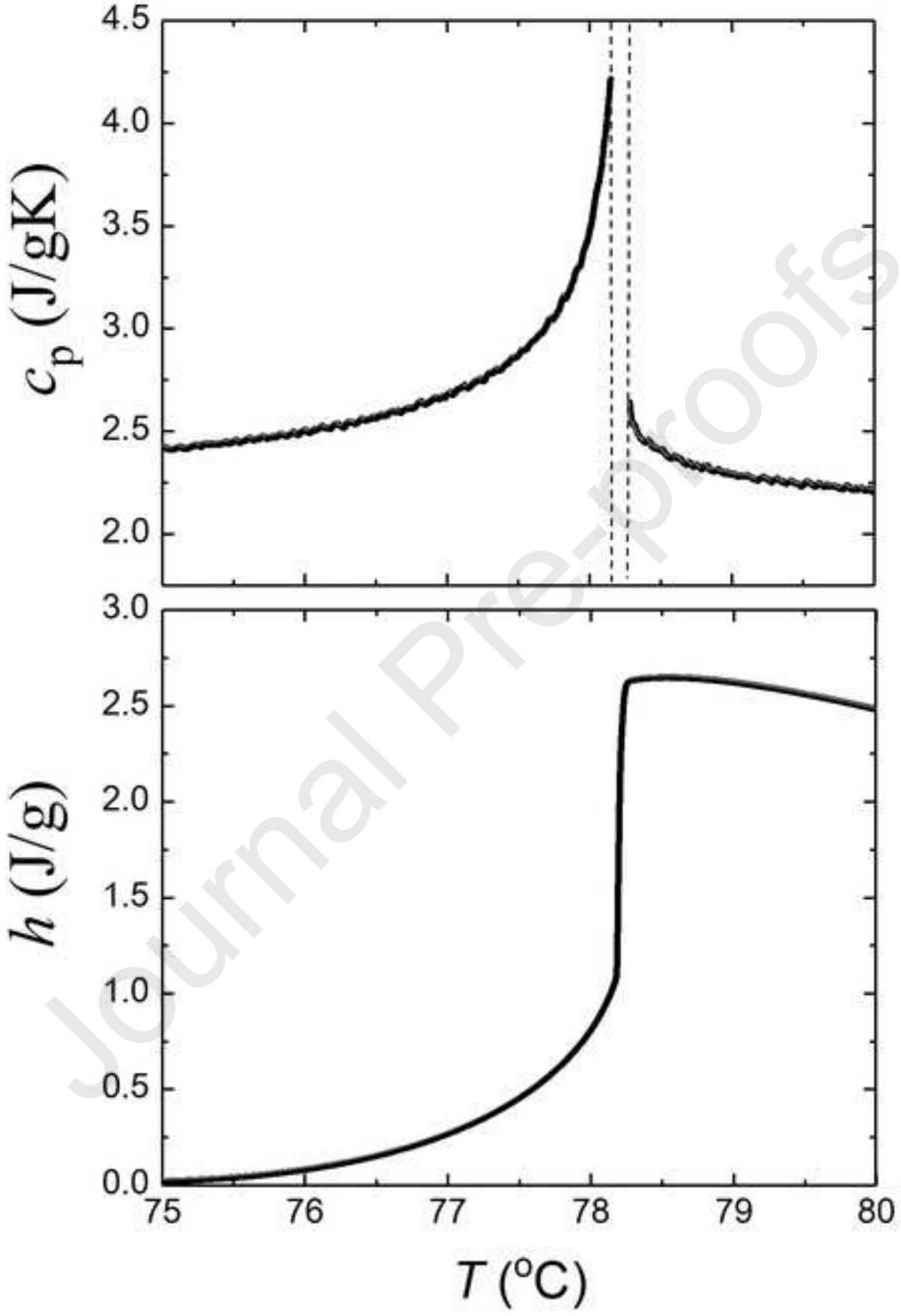

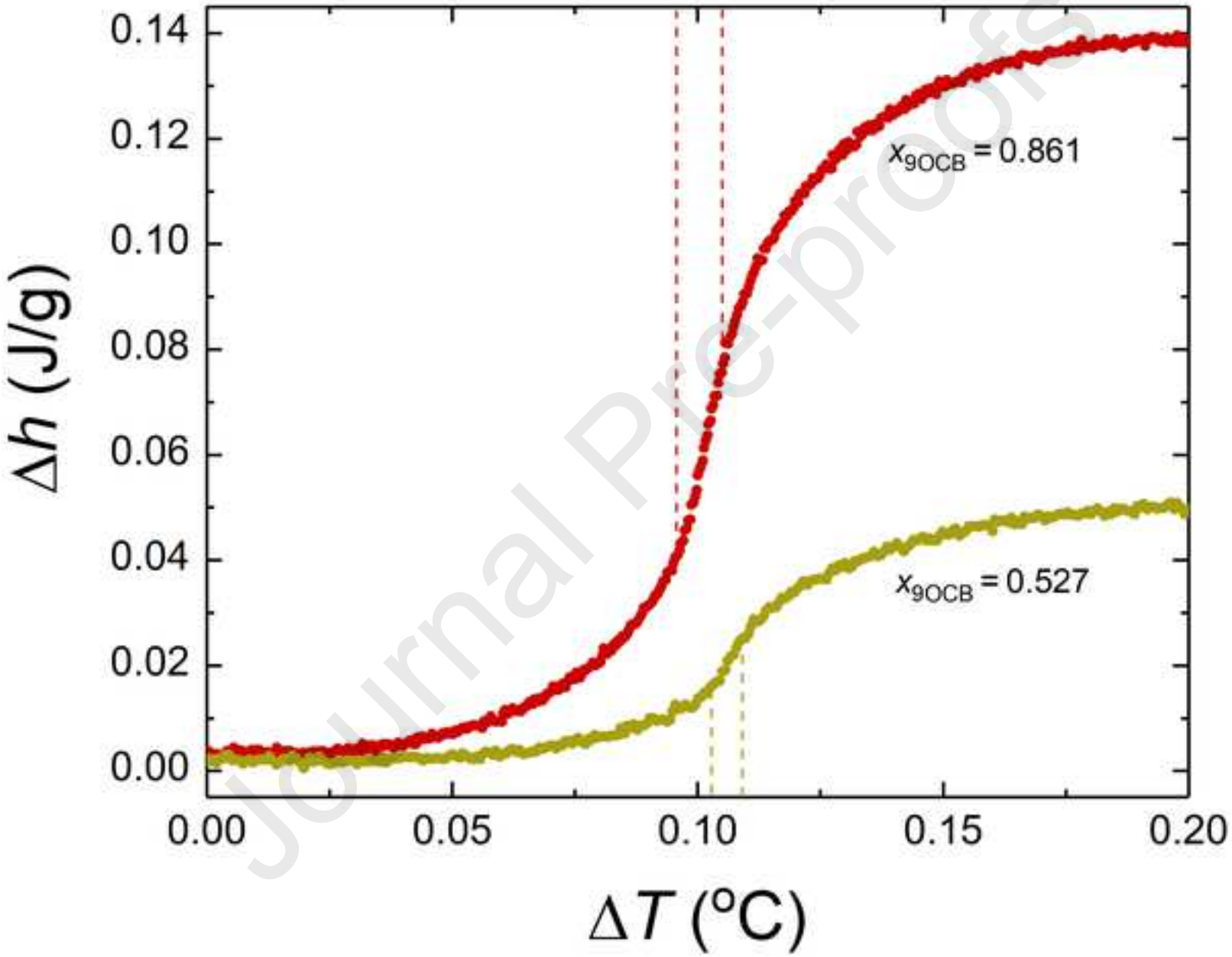

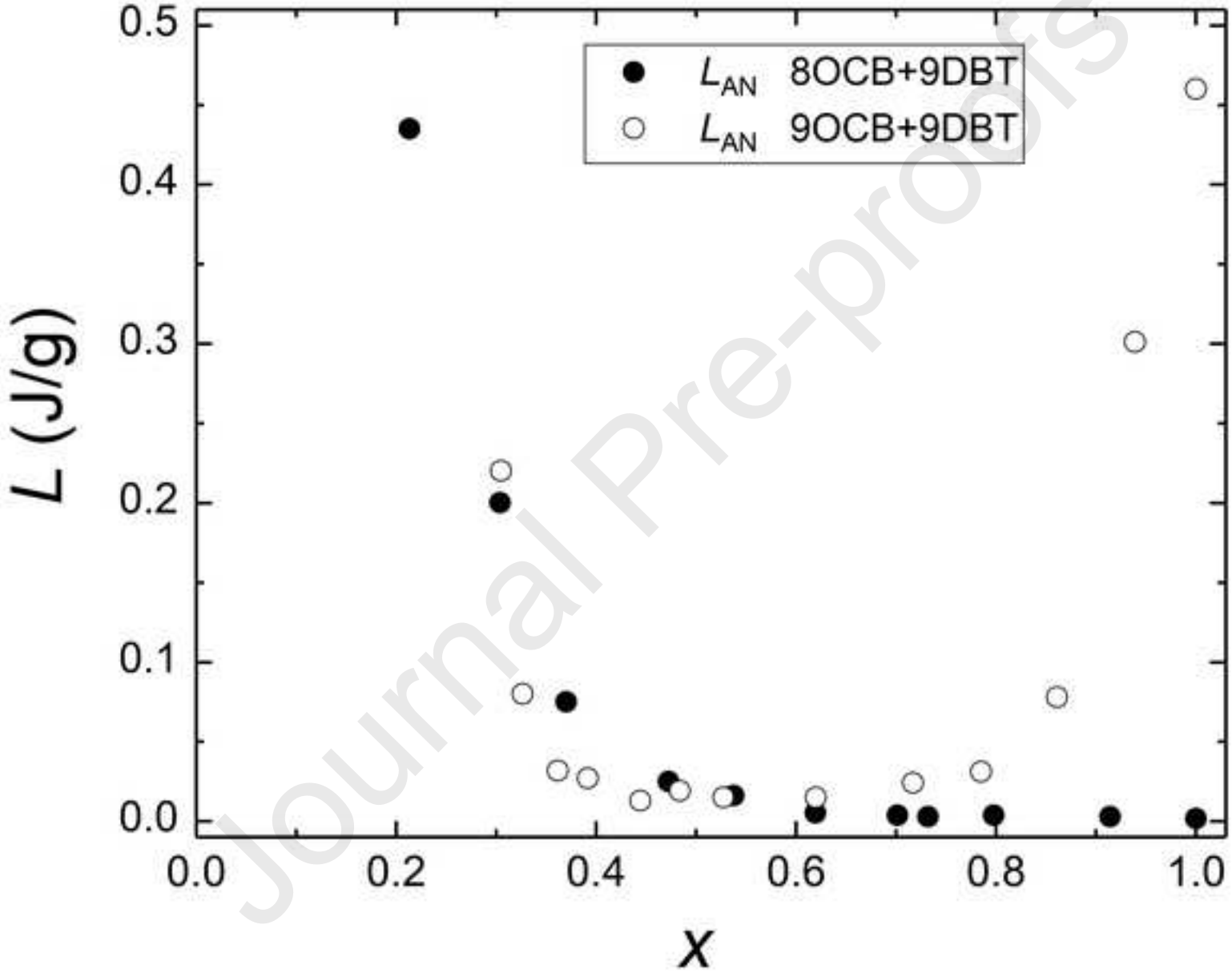

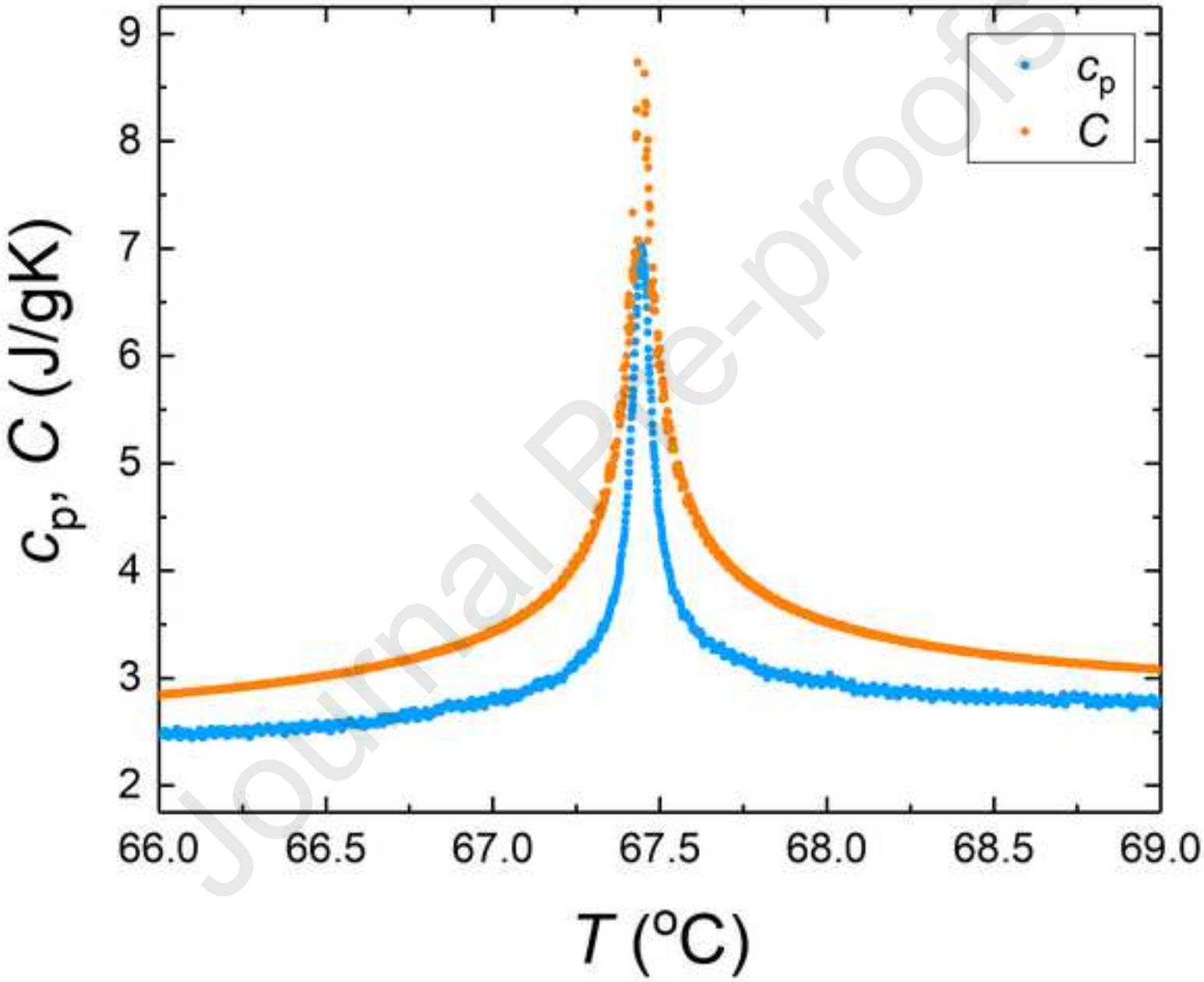

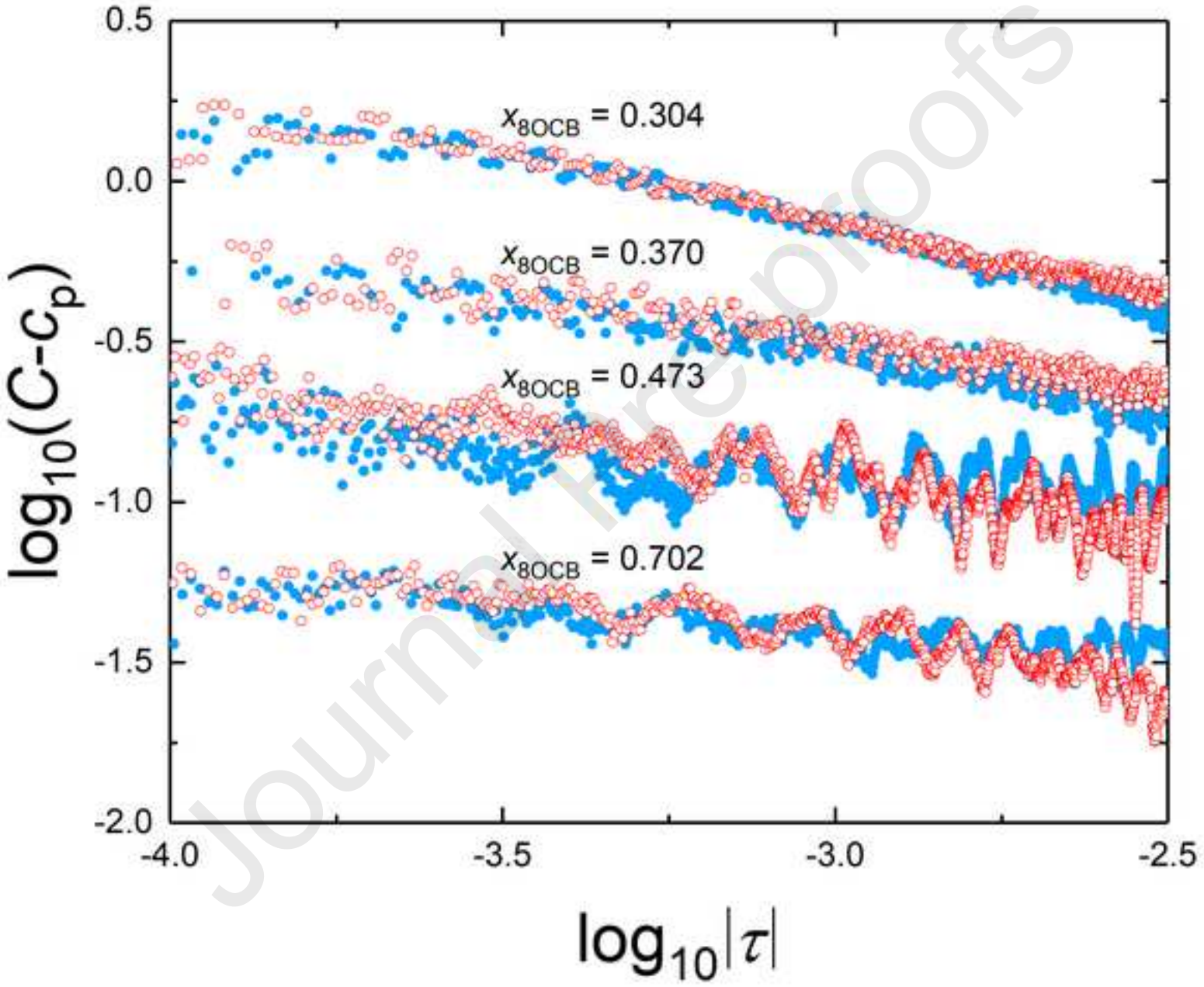

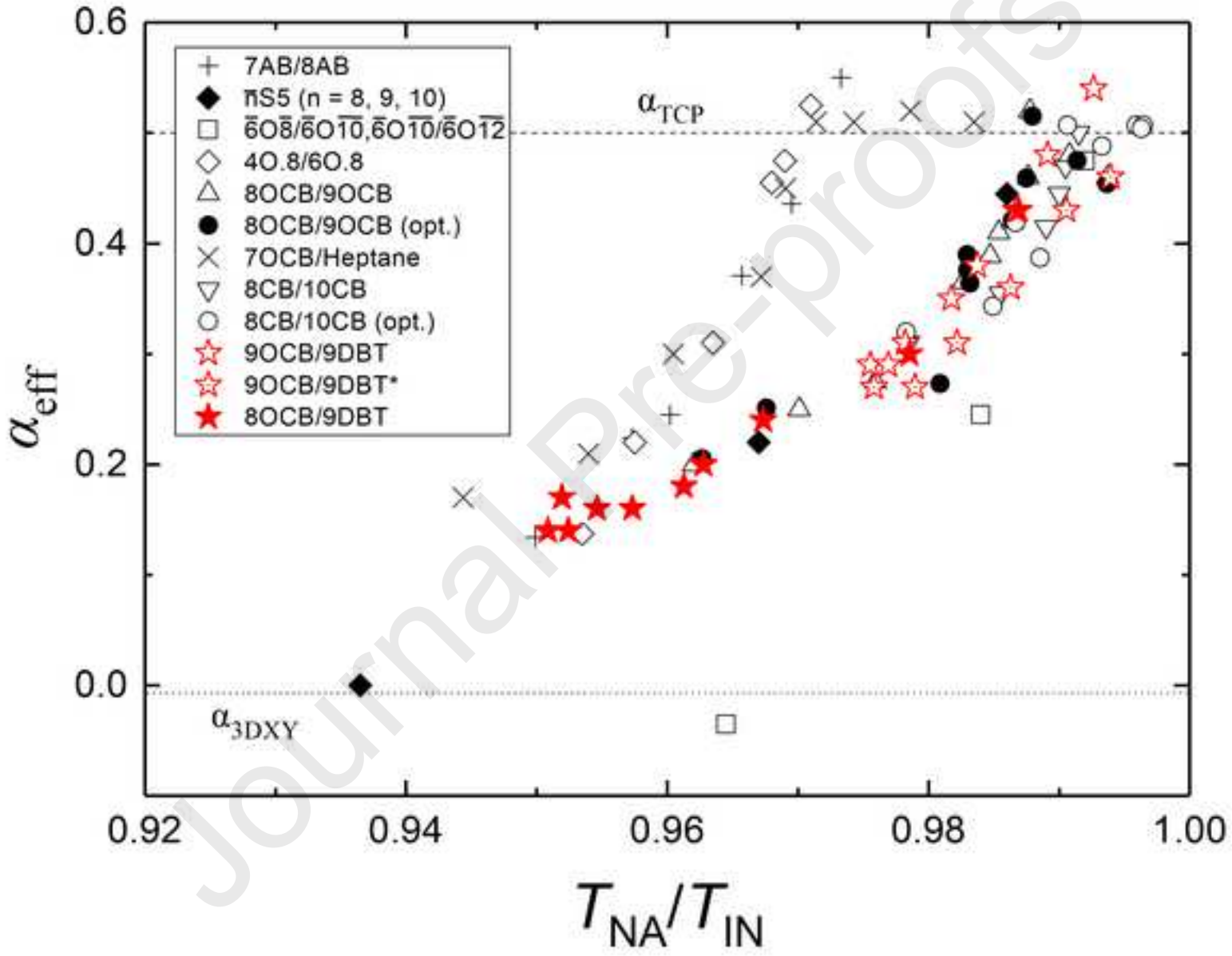

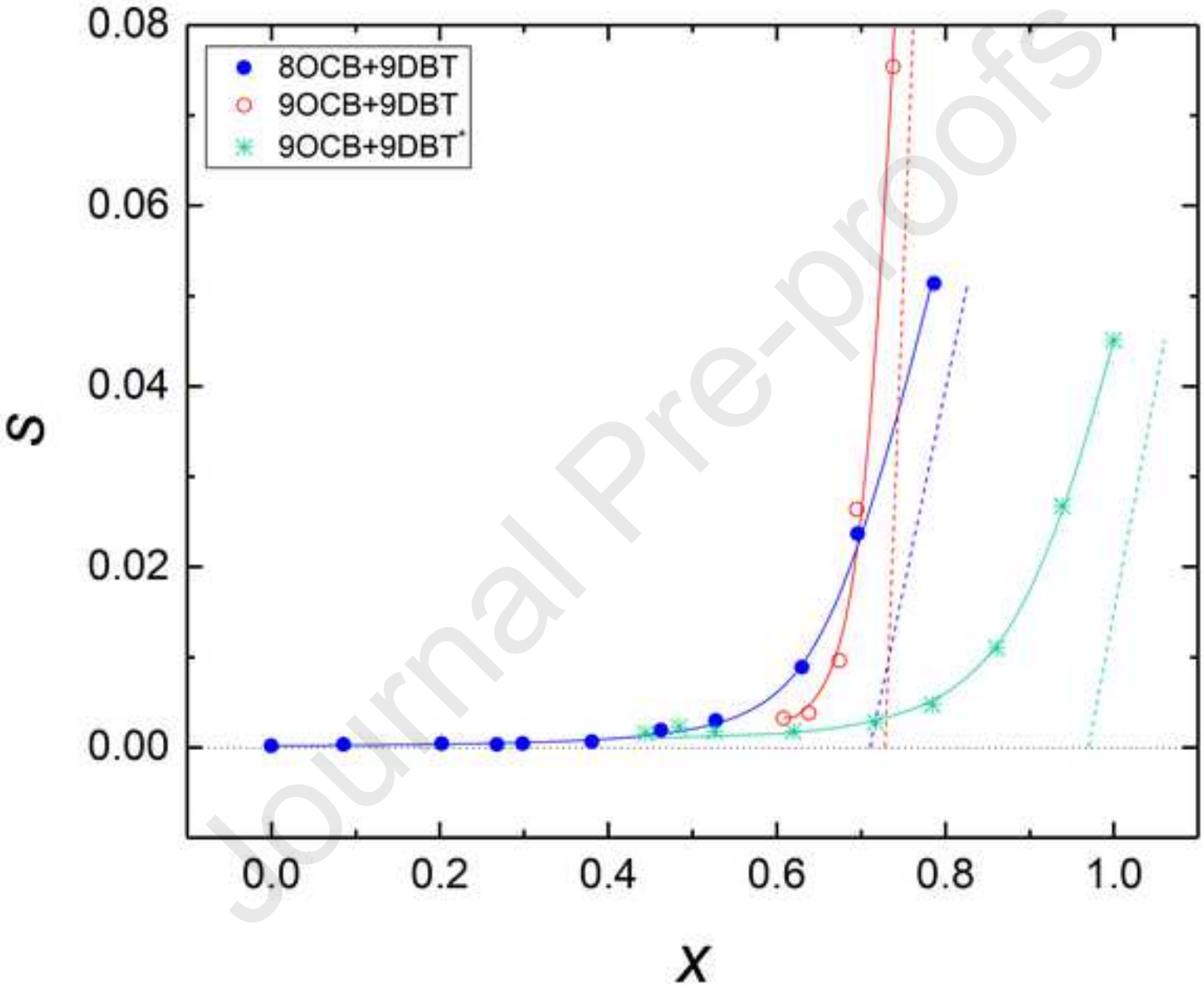

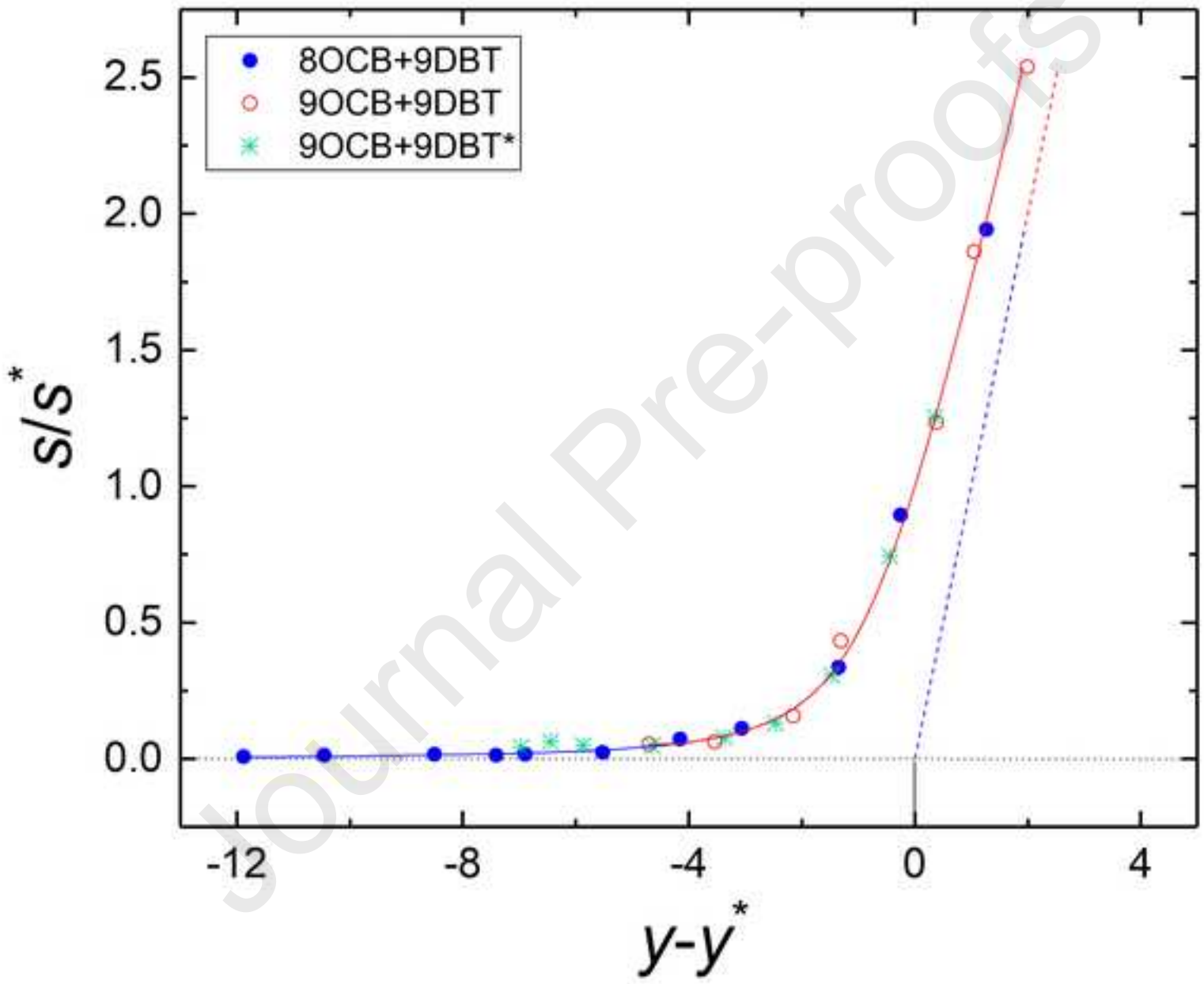

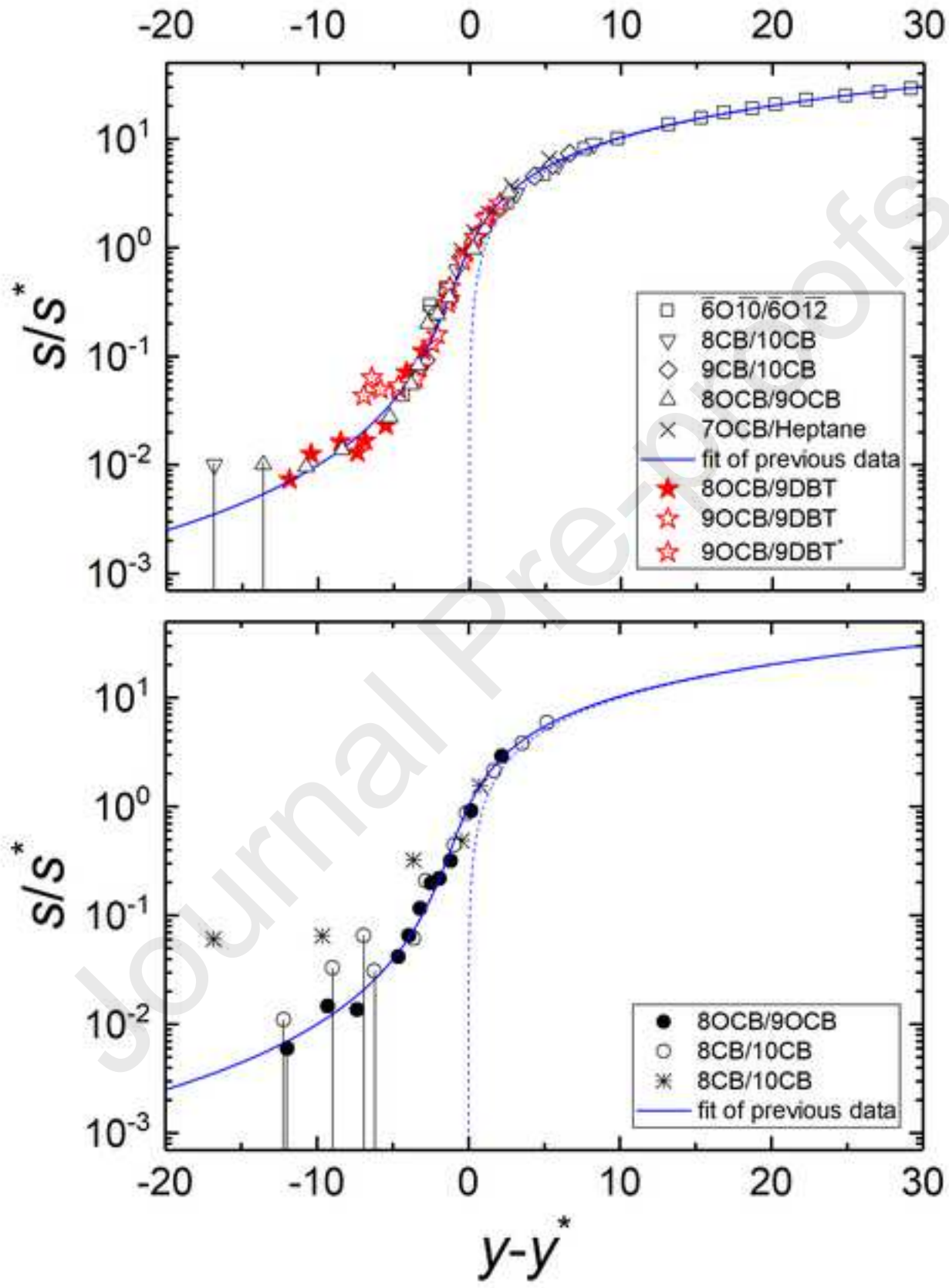

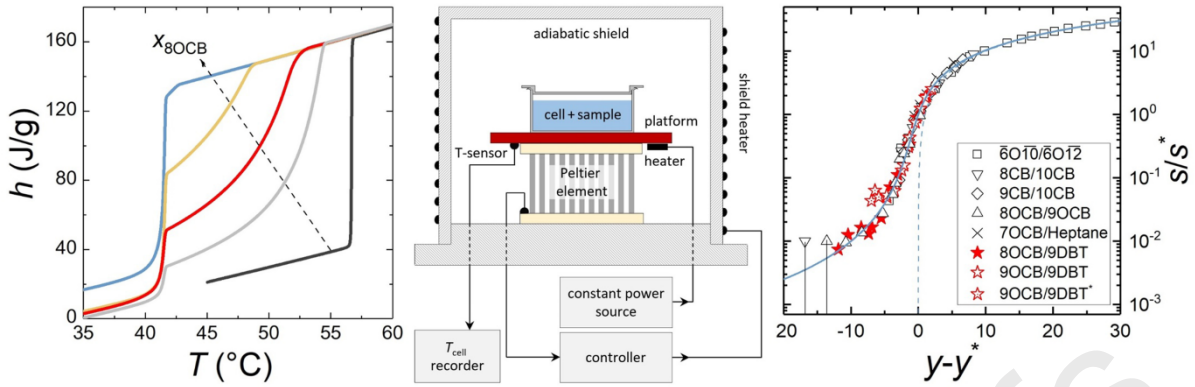


**HIGHLIGHTS**

- High-resolution Peltier-element-based adiabatic scanning calorimetry measurements
- Binary mixtures of two liquid crystal systems with enhanced nematic ranges
- Separation of latent heats for the eutectic and melting transitions
- Confirmation of the Halperin-Lubensky-Ma effect at smectic A-nematic transitions
- McMillan-ratio-dependence of critical exponent α of smectic A-nematic transitions